Characteristics of Particles Downstream of a Partially Failed Diesel Particulate Filter

A THESIS
SUBMITTED TO THE FACULTY OF THE GRADUATE SCHOOL
OF THE UNIVERSITY OF MINNESOTA
BY

Adam C. Ragatz

IN PARTIAL FULFILLMENT OF THE REQUIREMENTS
FOR THE DEGREE OF
MASTER OF SCIENCE

David B. Kittelson

December 2010

Acknowledgments

I am grateful to many individuals for their support during my graduate work at the University of Minnesota. First and foremost, I want to thank my advisor, Dr. David Kittelson, who provided years of guidance, technical advice, and intellectually stimulating discussions. I learned a great deal working with Dr. Kittelson. He both devised and inspired many novel experiments which I enjoyed working on, and he encouraged my curiosity no matter which direction it led.

I would also like to thank Dr. Winthrop Watts, who guided this research project, kept it on track, provided editorial advice, and helped elevate my writing abilities. I enjoyed especially lively academic discussions with Dr. Watts, and I appreciate the time he spent reading over many iterations of my graduate work.

On the fabled fourth floor of the Mechanical Engineering Department, I worked with many inspiring and marvelous students and professionals. They provided daily support, spent hours helping me set up experiments and gather data, and explained various data analysis techniques. A list of these friends and colleagues include: David Bennett, Anil Bika, Mark Brandl, Grace Chan, Aaron Collins, John Dixon, Marcus Drayton, Luke Franklin, David Gladis, Mike Gust, Jason Johnson, Matt Kenitzer, Andre Olson, Matt Schumacher, Jake Swanson, Dain Thule, and Darrick Zarling.

I also want to thank Dr. David Pui, Weon Gyu Shin, and Jing Wang. While working in Dr. Pui's lab, I gained a deeper understanding of the aerosol sampling instrumentation used in this study and how particles behave in these devices.

Without the generous financial support of Honeywell, this research project would not have been possible. I thank the Honeywell team, including Ryan Becker, Brian Krafthefer and Fouad Nusseibeh for providing equipment, data interpretation, sensor data processing, and technical support.

Finally, I would like to thank my friends and family members for their encouragement and support.

Abstract

A diesel particulate filter (DPF) can be used to reduce the particulate matter (PM) emissions from a vehicle. However, when these devices fail the tailpipe emissions can change. The main goal of this project was to determine if a soot sensor provided by Honeywell could detect a failed filter, defined as an exhaust aerosol concentration downstream of the DPF greater than the current US heavy duty PM standard of 13 mg/kWh (10 mg/bhp-hr). In this study a DPF failure was first simulated on an engine dynamometer test stand using an exhaust bypass valve. Then the valve was removed and the filter was actually failed in a series of steps by drilling out individual channel end caps.

Exhaust was cooled and diluted using a partial flow air ejector dilution tunnel, and dilution ratios were determined using raw and dilute nitric oxide (NO) measurements. Dilute diesel exhaust aerosol was characterized upstream and downstream of a DPF. Filter samples and an AVL photo-acoustic soot sensor were used to estimate PM mass emissions, and TSI aerosol instruments were used to measure aerosol size distributions and total number concentrations. An electrostatic precipitator, DMA, electrometer and CPC were used to evaluate the aerosol charge distribution. Downstream measurements were repeated as the filter was progressively failed in a series of steps.

These measurements were then used to evaluate the response of the Honeywell exhaust soot sensor. Under certain steady state conditions the sensor output showed a statistically significant increase as the filter was failed but the output was susceptible to interference from mechanical vibration and was dependent on engine operating conditions, and the exhaust system used. Exhaust aerosol charge measurements showed the concept is viable but further work is required to refine the sensor.

Table of Contents

List of Tables

List of Figures

List of Symbols

C_c	Cunningham slip correction
D_p	Particle diameter
e	Elementary charge (1.6×10^{-19} Coulomb)
L	Column length between exit slit and polydisperse aerosol inlet
μ	Gas viscosity
n	Number of elementary charges on the particle
q_a	Column aerosol flow rate
q_{sh}	Column sheath air flow rate
r_2	Outer radius of annular space
r_1	Inner radius of annular space
V	Inner collector rod voltage
Z_p	Electrical mobility

1. Introduction

Stringent regulations on tailpipe emissions from diesel powered vehicles continue to push engine designers to strive for innovative, emissions-reducing solutions. Table 1 shows the progression of federal regulations of carbon monoxide (CO), non-methane hydrocarbons (NMHC), oxides of nitrogen (NOx), and particulate matter (PM), over the past two decades that apply to heavy-duty diesel engines for on-road use (Code of Federal Regulations 40 CFR 86). European Union (EU) standards are also included for comparison (Euro 5 Regulation 83).

Table 1. US and Euro emission standards for heavy-duty engines [g/kWh (g/bhp-hr)]

	CO	NMHC	NOx	PM
US Model Year 1990	20.8 (15.5)	1.74 (1.30)	8.0 (6.0)	0.805 (0.60)
US Model Year 1991	20.8 (15.5)	1.74 (1.30)	6.7 (5.0)	0.335 (0.25)
US Model Year 1994	20.8 (15.5)	1.74 (1.30)	6.7 (5.0)	0.134 (0.10)
US Model Year 1998	20.8 (15.5)	1.74 (1.30)	5.4 (4.0)	0.134 (0.10)
US Model Year 2007 and Later	20.8 (15.5)	0.19 (0.14)	0.3 (0.2)	0.013 (0.01)
Euro V Started October 2008	1.5 (1.1)	0.46 (0.34)	2.0 (1.5)	0.020 (0.015)
Euro VI Starting January 2013	1.5 (1.1)	0.13 (0.10)	0.4 (0.3)	0.010 (0.007)

From 1998 to 2007 the US regulated levels of NMHC, NOx, and PM were reduced by 89%, 95%, and 90%, respectively. Current regulations have made it necessary for manufactures to use exhaust aftertreatment devices to maintain compliance (Eastwood, 2000; Johnson, 2009). One such device, a diesel particulate filter (DPF), is commonly used to meet the current diesel PM standard; however, this device can fail, reducing its effectiveness (Dabhoiwala et al., 2009). Diesel PM emissions are of concern because exposure is linked to potential adverse health effects (Dockery, 1993; HEI, 2003; Pope et al., 2004). The objective of this study was to characterize diesel exhaust aerosol upstream and downstream of both a new and failed DPF and use these data to evaluate the response of a Honeywell soot sensor. The soot sensor was designed to measure diesel PM in the raw exhaust, but it was unknown if the sensor would have the sensitivity to measure a DPF partial failure.

2. Background

2.1 Chemical and physical characterization of diesel PM

Unlike the other regulated constituents of diesel exhaust, PM is not defined chemically, but rather as the material collected by a filter during sampling after dilution and cooling to a temperature of 47+/-5°C or less (40 CFR 50). Engine-out PM emissions have a complex composition and structure, which typically consist of agglomerated carbonous material (soot) with adsorbed organic and inorganic compounds on the surface. Primary soot particles of diameter 15-30 nm form inside the combustion chamber in locally rich zones (Heywood, 1988; Maricq, 2007). Solid soot particles along with trace amounts of metallic ash derived from the lubrication oil are in the particle phase in the raw exhaust, while volatile constituents such as unburnt hydrocarbons and sulfates remain primarily in the gas phase until dilution and cooling where they can homogenously nucleate to form small volatile nanoparticles or adsorb on the surface of existing particles, growing them larger (Kittelson, 1998; Eastwood, 2000; Vouitsis et al., 2003; Burtscher, 2005; Maricq, 2007). The ratio of elemental carbon (EC), derived primarily from solid soot particles, to organic carbon (OC), derived primarily from unburnt hydrocarbons, can be determined by thermal analysis of a filter sample (Cadle et al., 1980; Huntzicker et al., 1982). For further information on the method used to analyze the filter samples reported in the results section, consult National Institute for Occupational Safety and Health (1998).

Figure 1 shows an idealized trimodal, lognormal size distribution of diesel aerosol particles, and identifies terms used in this paper (Cantrell and Whitby, 1978; Kittelson, 1998). Weightings of particle number, surface area, and volume are shown. The nucleation mode contains the majority of the particles by number. These nanoparticles are primarily composed of volatile hydrocarbons and sulfur-containing compounds, formed during the dilution and cooling process. The nucleation mode may also contain metallic ash and small solid carbon particles. The accumulation mode contains the majority of the particle surface area and mass. Accumulation mode particles are typically

chain agglomerates with adsorbed hydrocarbons, metallic ash, and sulfur-containing compounds on the surface. Coarse mode particles are formed when accumulation mode particles deposit on engine and exhaust system surfaces and later become re-entrained (Kittelson, 1998).

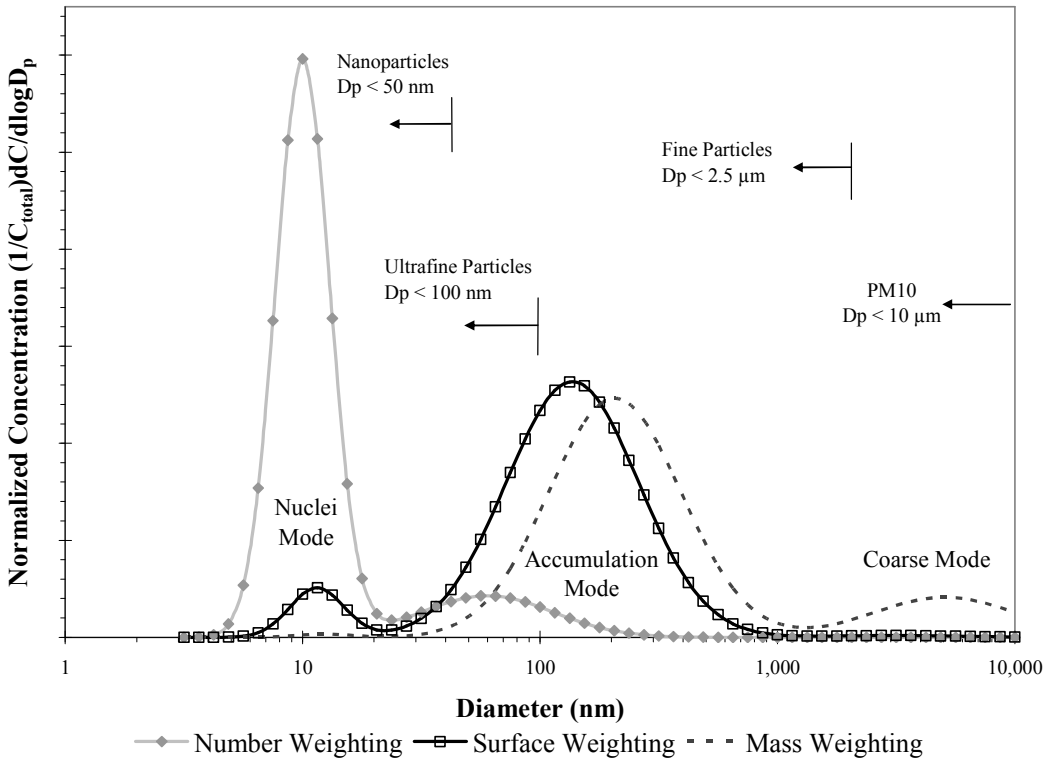

Figure 1. Trimodal size distribution

Source: Cantrell and Whitby (1978) as modified by Kittelson (1998)

Surface area and mass size distributions are constructed from particle size and number concentrations with the assumption of spherical particles. Knowledge of the particle density is required for construction of the mass size distribution. Since the particles being classified by electrical mobility diameter are assumed to be spheres when converting to a volume distribution, but may in fact not be, a size-dependent effective density can be used. A study by Park et al. (2003) used an aerosol particle mass analyzer (Ehara et al., 1996) to sample exhaust from a John Deere 4045 diesel engine similar to that used in this study and determine the size-dependent effective density. The study

found that effective density decreased with increasing particle size and is dependent on engine speed and load. The effective density found by Park et al. (2003) was used, when appropriate, for post-processing the data reported in the results section. By using a size-dependent effective density, the integrated mass from the number size distribution can be compared to the total mass determined by gravimetric analysis of the mass collected on a filter.

2.2 Exhaust aftertreatment

2.2.1 Diesel exhaust environment

Power output from a diesel engine is controlled by the amount of fuel injected rather than by throttling a premixed fuel-air mixture as in a spark ignition engine. This results in a wide range of fuel-air ratios with an overall heterogeneous and lean mixture, creating an oxidizing environment in the exhaust (Heywood, 1988; Stone, 1999). Diesel exhaust temperatures are generally lower than spark ignition engine exhaust temperatures partially due to their higher thermal efficiency and dilution from excess air (Eastwood, 2000). Exhaust temperatures are typically 200°C to 500°C, often tending toward the lower end of this range, especially for urban and light load drive cycles (Adams et al., 1996; MacDonald and Simon, 1988). Within this range temperature changes can be rapid and aftertreatment devices must be resistant to thermal fracture.

2.2.2 Diesel oxidation catalyst (DOC)

Diesel oxidation catalysts are typically constructed as metal or ceramic flow-through devices with a square matrix or honeycomb structure to increase surface area. The walls are coated with a washcoat and an oxidation catalyst(s), usually a precious metal (Eastwood, 2000; Heywood, 1988). An appropriately sized device, with sufficient surface area and residence time for the exhaust gases to interact with the catalyzed wall, can substantially reduce CO and HC emissions as well as remove heavier HC which would have become adsorbed volatile material on the surface of PM during dilution and

cooling (Eastwood, 2000). These constituents are removed by oxidation and relevant global reactions are shown in Equation 1.

$$CO + \tfrac{1}{2}O_2 \Rightarrow CO_2$$
$$C_xH_y + (x+\tfrac{y}{4})O_2 \Rightarrow xCO_2 + (\tfrac{y}{2})H_2O$$

Equation 1. Oxidation reactions for CO and HC

A DOC can reduce CO, HC, and volatile PM emissions, but it is relatively ineffective against solid particulate matter such as black soot and metallic ash, which flow through the device unaffected.

2.2.3 Diesel particulate filter (DPF)

As the name implies, a DPF removes diesel PM from the exhaust stream by filtration while allowing gaseous emissions to pass through. Though a variety of DPFs exist, this study focuses on the ceramic wall flow filters. Figure 2 shows a ceramic monolith with alternate channels blocked in a checkerboard pattern (Howitt and Montierth, 1981). Exhaust enters an open channel with a blocked exit. Gaseous emissions flow through the wall and exit through an adjacent channel, while solid PM is filtered at the wall.

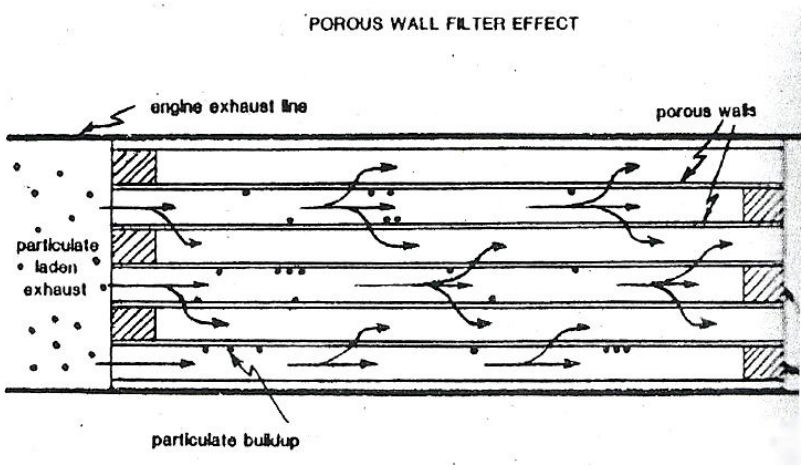

Figure 2. Porous wall flow DPF

Source: Howitt and Montierth, 1981

As PM is trapped on the walls it forms a soot cake which improves filtration efficiency and leads to higher backpressure as the filter loads (Howitt and Montierth, 1981). Excessive soot buildup can lead to exhaust backpressures which hinder the performance of the engine and in extreme cases, cause it to stop completely. Therefore, the filter must be regenerated "cleaned" to remove the soot. Black carbon will begin to oxidize in the presence of excess oxygen at 550°C to 600°C but these exhaust temperatures are rarely achieved (Eastwood, 2000). The filter can be heated with electric heaters or by injecting excess fuel into the exhaust to reach temperatures high enough to combust the soot in a process know as active regeneration. Alternatively, it has been shown that NO_2 has the ability to oxidize soot at much lower temperatures, around 265°C (Cooper and Thoss, 1989). Usually the majority of engine-out NO_x emissions are in the form of NO but the NO_2/NO ratio can be increased by first exposing the exhaust to a DOC where NO is oxidized to NO_2 in the presence of excess oxygen (Cooper and Thoss, 1989). This configuration, known as passive regeneration, allows the filter to continuously regenerate at lower temperatures. For this study, a DOC followed by a DPF supplied by Donaldson Company was used.

2.2.4 Modes of DPF failure

There are three basic DPF failure mechanisms which were considered. Thermal separation is a failure process where the DPF pulls away from its metal housing allowing exhaust to flow around the outside of the filter. Ring cracking is perpendicular to the flow through the DPF and allows exhaust to enter an open channel and exit an open channel without flowing through the wall. Catastrophic regeneration occurs when the regeneration temperature becomes large enough to melt the filter, creating holes where exhaust is free to flow through the trap without being filtered. For this study, the filter was failed in a series of steps by drilling out end-caps on the downstream side of the DPF. This method was easy to quantify and allowed a large range in failed filter area, mimicking everything from a small crack up to a very large failure to be evaluated. The condition of a DPF is typically monitored by the pressure drop across it, to get an

estimate of soot loading. However, studies have shown that a pressure sensor alone is not enough to detect a trap failure (Nieuwstadt and Trudell, 2004).

2.3 Real-time exhaust PM sensors

Both the Code of Federal Regulations (40 CFR §86.010-18) and the California Code of Regulations (Title 13 Section 1971.1) state that an on-board diagnostic (OBD) monitoring system for on-road heavy-duty diesel engines shall detect a malfunction with a PM threshold of 0.04 g/kWh (0.03 g/bhp-hr). This value determines the required sensitivity of an OBD sensor if the desired purpose is to detect a malfunction and report this information to the operator, usually through an engine light fault indicator. A number of attempts to accurately and continuously measure exhaust PM levels in real-time have been made. Some have succeeded but none with the accuracy, repeatability, robustness and cost-effectiveness to set one idea apart from the rest. The following is a short summary of relevant sensor concepts.

Spark discharge soot sensors (SDSS) are a combination of conventional spark and glow plugs. This provides a low cost way of monitoring a DPF but such sensors are dependent on a large number of parameters, including exhaust gas velocity, temperature, pressure, moisture content, and particle concentration. SDSS are susceptible to fouling from particles depositing on the surface and they do not perform well when exhaust temperatures rise above 350°C (Gheorghiu, 2006). This type of sensor may perform well in certain situations where temperatures are low and conditions are well characterized.

The University of Texas at Austin has designed a sensor consisting of two electrodes immersed in the exhaust stream. One electrode is charged to a high voltage while the other is connected to a charge amplifier. Researchers at UT Austin believe charge-carrying particles entering the electric field of the first probe alter the charge state of the second probe in proportion to the concentration of carbonous material in the exhaust (Diller, 2008). This sensing concept shows promise but is still in the research phase.

The Dekati Electrical Tailpipe PM Sensor (ETaPS) is another particle charge based measurement. This device contains a corona discharge needle within a charge cage which is connected to an electrometer. The cage has perforated walls and allows exhaust to freely flow past the charging section. If particles are present in the exhaust stream they will pickup a charge in the charging section and the electrometer will measure a net flow of current leaving the cage (Dekati, 2008).

GE Sensing & Inspection Technologies announced the release of the ACCUSOLVE Advanced Diesel Particulate Filter Soot Sensor in the spring of 2009. This sensor uses radio-frequency (RF) technology to measure the amount of soot loading within a DPF. Since RF energy is absorbed by soot the amount of soot loading in a ceramic filter can be determined by the degree of signal attenuation. This technology has been described before by (Walton et al., 1991). Although this technique can accurately measure the amount of soot loading within a DPF it does not measure soot emissions. This technology has application helping the engine control unit (ECU) determine when to use active regeneration, but is only able to measure the instantaneous amount of soot contained within the DPF and not the amount of material leaving the downstream side of the filter.

A sensor to directly detect the soot emissions after a DPF has been designed by Bosch of Germany (Ochs et al., 2010). The exhaust gas sensor for particulate matter (EGS-PM) has a soot particle sensing element consists of two inter-digitated comb-like electrodes with an initially infinite electrical resistance. In the presence of exhaust PM, particles are collected onto the electrodes forming a conductive path between the fingers leading to a drop of the electrical resistance. The rate of drop in resistance depends on the concentration, size, and composition of the particles present in the exhaust. The sensor can be regenerated by heating to over 600°C and burning off the soot deposits. If this sensor can prove to be reliable and repeatable over the life of a DPF and produce results which correlate well with a known standard measurement of soot, such as gravimetric filter analysis, it could show promise.

Building off of earlier work by Ricardo & Co. Engineers Ltd., (Kittelson and Collings, 1987) investigated a fast-response electrostatic particle sensor capable of measuring changes in the net charge of diesel exhaust over one engine cycle. They found that a spike in net charge was associated with each exhaust blow-down event. The probe was immersed in the exhaust flow and electrically isolated from its surroundings and an electrometer was used to amplify the signal. The magnitude and polarity of these spikes changed with engine load and speed and varied from engine to engine. Though the origin of the signal was not fully understood, the results were intriguing because the probe required to make these measurements was compact and inexpensive. It was hypothesized by (Kittelson and Collings, 1987) that the origin of the signal was a combination of flame ionization during combustion and surface interactions during the blow-down process. However, more work needs to be done on the natural charge of diesel exhaust to better understand this signal.

A joint effort by the University of Minnesota and Honeywell Inc., aimed to further investigate the concept described by (Kittelson and Collings, 1987). The project was initially funded by the Department of Energy (DOE) in 2001. The main objectives of this project were to develop, test and deliver a working prototype of a low cost, high speed, reliable sensor which was capable of operating in the harsh environment of diesel exhaust. The project succeeded in delivering a working sensor capable of measuring charge spikes from individual cylinders on a variety of engines. An extension of this project looked at the natural charge distribution of diesel exhaust using the concept of tandem differential mobility analyzers (TDMA). This method of analyzing exhaust charge has been reported elsewhere (Moon, 1984; Kim et al., 2005 and Maricq, 2006). The findings were similar in that all reported the diesel aerosol charge distribution roughly followed a high temperature Boltzmann distribution. However, (Maricq, 2006) reported the net charge to be neutral, and (Kim et al., 2005) showed a slight negative net charge. The Honeywell sensor work reported by (Dixon, 2007) showed a net positive charge at low engine loads but a net negative charge at high engine loads.

In 2008, the California Air Resourses Board (CARB) funded a project (ICAT Grant 07-4) to look at the sensors response in the post-DPF environment. That work is presented in this Master's Thesis. The main objective of this project was to characterize diesel exhaust aerosol upstream and downstream of a new and failed DPF and to use these data to evaluate the response of the Honeywell soot sensor. Figure 3 shows one of the sensors which was used in the study starting in 2008 along with the proprietary electronics used by Honeywell for amplifying the signal. The sensor is in the lower right followed by the smaller electronics box containing an amplifier which then sends a signal to the larger electronics housing for the final stage of amplification and data acquisition.

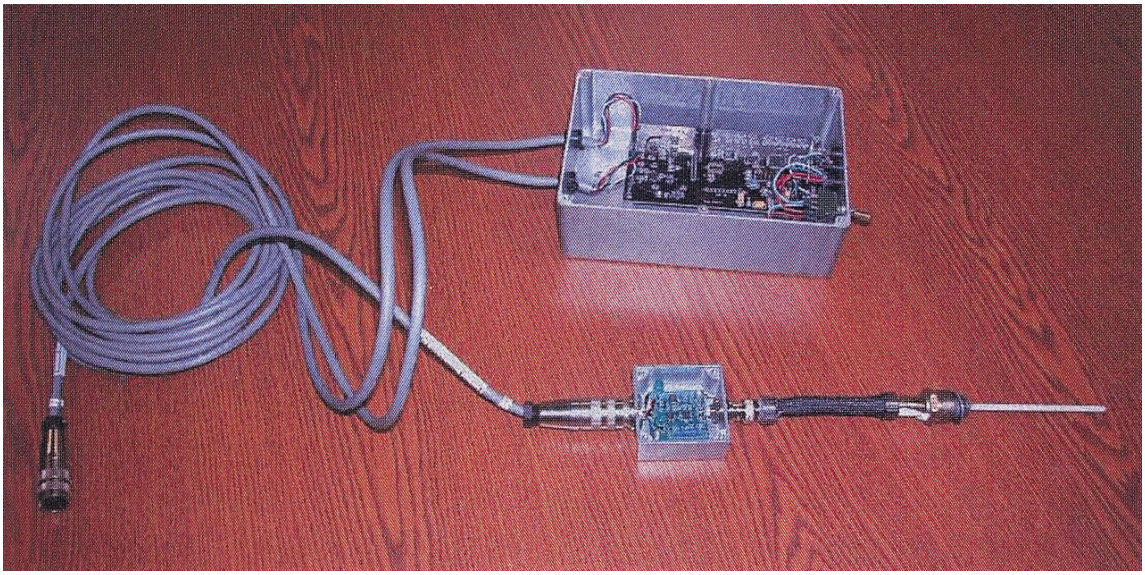

Figure 3. Honeywell sensor, preamp and secondary amplifier

3. Experimental apparatus

3.1 Engines and exhaust aftertreatment

For the evaluation of the Honeywell soot sensor a modern diesel engine with the capability of exceeding the on-road OBD emission standard at certain conditions was desired. Previous work on a John Deere 4045H diesel engine showed that the engine emissions were suitable for this project and well documented for comparison. A short summary of previous work is shown in Appendix B. Due to an unexpected dynamometer

failure a second engine was used for some of the tests where special care was taken to closely match the soot output from the previous engine.

The first test engine was a 4-cylinder, 4.5-L, 129-kW (173 hp) at 2400 RPM, model year 2005, John Deere 4045H. The engine is turbocharged, aftercooled with common rail fuel injection, and has EPA tier 2 approval for off-highway applications. Exhaust gas recirculation was not setup on this engine. API-CJ-4 engine oil is recommended for use with exhaust filtration devices and was used during testing. The oil was broken in for over 10 hours at various engine load and speed conditions. The engine is equipped with a Donaldson crankcase filtration system and filtered crankcase fumes are vented to the atmosphere rather than introduced back into the engine. The engine was fueled with ultra-low sulfur diesel (ULSD) fuel and operated on a DC electric dynamometer test stand.

The second test engine was a 4-cylinder 5.2-L, 142-kW (190 hp) at 2600 RPM, model year 2005, Isuzu 4HK1-TC. The engine is turbocharged, aftercooled with common rail fuel injection, and meets EPA requirements for model year 2004 heavy-duty truck engines for on-road applications. Exhaust gas recirculation was connected and controlled by the stock engine control module. API-CJ-4 engine oil was used and broken in for approximately 10 hrs before testing began. The engine was fueled with ultra-low sulfur diesel (ULSD) purchased from a local SuperAmerica gas station.

The same Donaldson catalyzed filter (part # 226355-016-190; 26.7 x 35.6 cm) was used for both engines and is capable of handling the total exhaust flow from an engine up 300 HP (Donaldson, 2008). This was used with an existing, Donaldson style 3, aftertreatment system that included a catalyzed pre-filter (part # P229063) and two end cones. The new filter replaced an identical filter that had been used by UMN for another project. The exhaust filtration system is modular in design and allows for swapping in and out of the individual sections.

3.2 Instrumentation

3.2.1 Electrometer

The TSI model 3068A Aerosol Electrometer is designed to measure the net charge on aerosol particles in the size range of 2 nm to 5 μm. It consists of a current sensor, an absolute filter mounted on a Teflon insulator within a metal housing and a solid state electrometer operational amplifier. Particles are collected on the absolute filter as the aerosol sample is passed through the instrument. The metal housing around the filter acts as a Faraday cage and current coming from ground to neutralize the effect of these charged particles is measured. The current sensor is capable of measuring from 0 to 10 pA with an accuracy of 2 fA. The 3068A has a maximum flow rate of 10 L/min.

3.2.2 Particle counters

A TSI 3025A butanol based condensation particle counter (CPC) was used to determine the aerosol particle number concentration (part/cm^3). The 3025A covers the size range from 2.5 nm to 1,000 nm in diameter up to a concentration of 10^5 part/cm^3. The 3025A works by splitting the incoming flow so a known fraction of the sample stream passes over a heated pool of liquid alcohol. The sample then flows through a cold condenser tube and the saturated alcohol vapor condenses on the particles as the sample is cooled. The droplets are grown to an optically detectable size and counted by an optical particle counter. This process is discussed in greater detail elsewhere (Sinclair and Hoopes, 1975; Agarwal and Sem, 1980).

3.2.3 Classification by electrical mobility

A differential mobility analyzer (DMA) was used to classify particles by their electrical mobility. The DMA is discussed in greater detail than the other instrumentation in this section because it was used in a different way than the standard TSI configuration for part of the testing, and requires a greater understanding to effectively interpret the results. The DMA used in this investigation has two concentric cylinders with an air gap

in between. Sample aerosol is introduces through a small opening on the outside wall with a sheath of clean air running along the inside. A voltage is applied to the center rod with respect to the grounded, outer wall. A positive voltage on the center rod will draw negative particles closer and repel positive ones. The opposite is true when the polarity is switched. Figure 4 shows the internal flow path within the DMA.

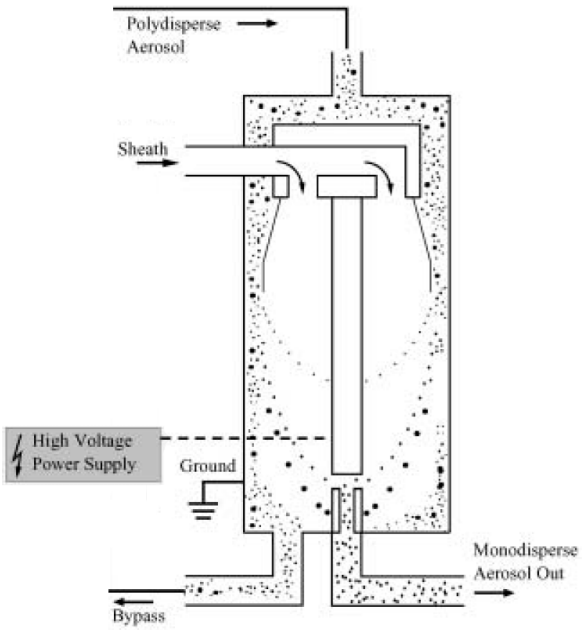

Figure 4. DMA flow path

Source: TSI, 2003

Particles entering the DMA through the polydisperse aerosol inlet can have a wide range of electrical mobilities. In a typical application the flows are held constant and the voltage on the center rod is adjusted so charged particles with a specific, narrow band of electrical mobilities, exit through the monodisperse outlet. For this investigation a recirculation loop was used which cleans the bypass flow and ensures the sheath and bypass flows are equal and therefore, the polydisperse and monodisperse flows will also be equal. When these criteria are met Equation 2 describes the relationship between electrical mobility and classifier parameters. Further explanation can be found by (Knutson and Whitby, 1975).

$$Z_p^* = \frac{q_{sh}}{2\pi VL} \ln\left(\frac{r_2}{r_1}\right)$$

Equation 2. Electrical mobility related to classifier parameters

For a given column such as the TSI 3081 Long DMA used in this investigation the geometric parameters are fixed and a flow controller maintains a constant sheath flow rate. Therefore, the selected electrical mobility is determined by the voltage on the center rod. Equation 3 shows the electrical mobility for a spherical particle (Hinds, 1999).

$$Z_p = \frac{neC_c}{3\pi\mu D_p}$$

Equation 3. Particle electrical mobility

Assuming the mean free path inside the column remains constant, which is a good assumption with constant temperature and pressure, the Cunningham slip correction C_c is a function of particle size. Setting Equation 2 and Equation 3 equal to each other and rearranging yields Equation 4.

$$\frac{D_p}{C_c} = \frac{2neVL}{3\mu q_{sh} \ln\left(r_2 / r_1\right)}$$

Equation 4. Particle diameter as a function of classifier parameters

Under constant temperature and pressure the viscosity will also remain constant. Therefore, with a constant sheath flow Equation 4 shows particle size as a function of center rod voltage, the number of charges on a particle and known constants. Liu and Pui (1974) discuss how a bipolar charger or neutralizer can be used to put a predicted amount of charge on the incoming polydisperse sample. Appendix A shows the fraction of particles carrying -6 to +6 charges base on equations by (Wiedensohler and Fissan, 1988) and (Gunn, 1956). If the charge distribution after the sample passes through the neutralizer is known then the equation above relates column voltage to monodisperse particle size. The electrostatic classifier with a neutralizer and a CPC can be used to measure the number concentration of particles in a specific size range. The width of this

window depends on the transfer function which was derived by (Knutson and Whitby, 1975). Equation 5 gives the width of the base of the transfer function.

$$\Delta Z_p = \frac{q_a}{q_{sh}} Z_p^*$$

Equation 5. Mobility bandwidth

The transfer function predicts the probability of a particle with a given electrical mobility exiting the monodisperse outlet for a given set of parameters (Knutson and Whitby, 1975). The voltage on the column can be ramped continuously and CPC counts can be binned by size to create a number size distribution. This configuration is commonly referred to as a scanning mobility particle sizer (SMPS™). The SMPS was operated with a sheath flow rate of 10 L/min allowing it to size particles from about 8 nm to 300 nm with a 60 s up scan and a 30 s down scan yielding a response time of 90 s.

Alternatively, the neutralizer can be removed and the voltage can ramped continuously while the CPC and electrometer are simultaneously monitoring the monodisperse outlet. In this configuration the DMA is classifying particles by electrical mobility and the ratio of the electrometer to the CPC gives the natural charge per particle for a range of electrical mobilities.

3.2.4 Electrostatic precipitator

An electrostatic precipitator can be thought of as a DMA with only one inlet and one outlet. The voltage on the center rod was set high enough that all particles carrying a charge would be lost to the wall. The center rod was charged with +7kV so negatively charged particles would be attracted and collide with the center rod and the outer wall was grounded, attracting positively charged particles which are repelled by the center rod. The electrostatic precipitator used was similar in design to (Jung et al., 2005) and was used to determine the fraction of particles caring a charge. An SMPS was placed downstream of the electrostatic precipitator. With the device turned off a typical size distribution was taken. Then with the device turned on another size distribution was taken. The second distribution only contained the neutral particles which passed through

the electrostatic precipitator without removal. From the difference of the two size distributions one can determine the size-dependent charge fraction. This result was then compared to a high temperature Boltzmann equilibrium charge distribution.

3.2.5 Engine exhaust particle sizer

A TSI 3090 Engine Exhaust Particle Sizer (EEPS™) was also used to measure particle size distributions. Like the SMPS the EEPS has a column where particles are separated by electrical mobility. However, instead of counting these particles with a CPC the outside wall of the column in the EEPS consists of an array of electrometers which constantly measure current as charged particles impact. Since the EEPS monitors all size bins continuously it is much faster than the SMPS. The EEPS sizes particles from 5.6 to 560 nm with a 1 s response time. The EEPS has been included for comparison, but the primary focus of this study will remain on results obtained with the SMPS. Further explanation on the operation of the EEPS can be found in (Kittelson et al., 2006; TSI, 2006).

3.2.6 Mass measurement

Honeywell provided an AVL Micro Soot Sensor, Model 483 that relies on the photoacoustic measurement method. Diesel exhaust contains strongly absorbing soot particulates that are exposed to modulated light. The periodical warming and cooling of the black carbon particles and the resulting expansion and contraction of the carrier gas results in a sound wave that is detected by means of microphones (AVL, 2004). The AVL has a range of detection from 1 $\mu g/m^3$ to < 50 mg/m^3 $\pm$ 10 $\mu g/m^3$ with a drift of 10 $\mu g/m^3$/hr of operation. The AVL sensor has its own dilutor capable of 20:1 dilution.

Gravimetric filter measurements were also made during testing. Samples were collected on 47 mm Teflon filters at a flow rate of 72 L/min. Filters were weighed using a Cahn Microbalance and values reported are the average of 4 filters at each condition.

3.2.7 Gas analyzers

The total dilution ratio (DR) when sampling exhaust was determined by measuring the raw exhaust NO concentration and the NO concentration in the diluted sample. Raw exhaust was transferred using a heated line to a CAI gas analyzer. Dilute NO measurements were made with a Horiba CLA-510SS. Gas analyzers were zeroed and spanned daily to ensure an accurate measurement.

3.3 Dilution system

Measurements were made using a two stage ejector dilutor system. This system is similar to those described previously (Abdul-Khalek et al., 1999), and extensively evaluated during the Coordinating Research Council (CRC) E-43 project (Kittelson et al., 2002). Exhaust enters the system through a 5-cm long, 0.64-cm diameter stainless sampling probe immersed in the exhaust flow, and passes through a short section (6.35-cm) of stainless steel tubing referred to as the transfer line (TL). An Air-Vac TD-190 or TD-110 air ejector pump with a critical flow orifice provided the first stage of dilution. The system was designed to give a primary dilution ratio (DR) ranging from 5 to 25:1 with a regulated, total dilute exhaust mixture flow rate of 100 - 200 L/min. It is critical that the orifice not be allowed to plug with soot as this will increase the DR and impact the resulting measurements. Ultra-clean compressed air was provided by a Donaldson pressure swing adsorption system. Diluted aerosol then passed into a heated residence time chamber with an internal flow distribution cone. The chamber was designed for a residence time of 1 s at 100 L/min. Residence time chamber temperature was kept at 47$\pm$3 C. Pressures and temperatures were measured in the residence time chamber as well as in the exhaust. After the residence time chamber an optional secondary dilution took place using another TD110 air ejector. Figure 5 is a schematic of the entire sampling system with instrumentation. Note that the TL is not shown in the schematic to illustrate the point that the tunnel may be placed up- or downstream of the exhaust filtration system.

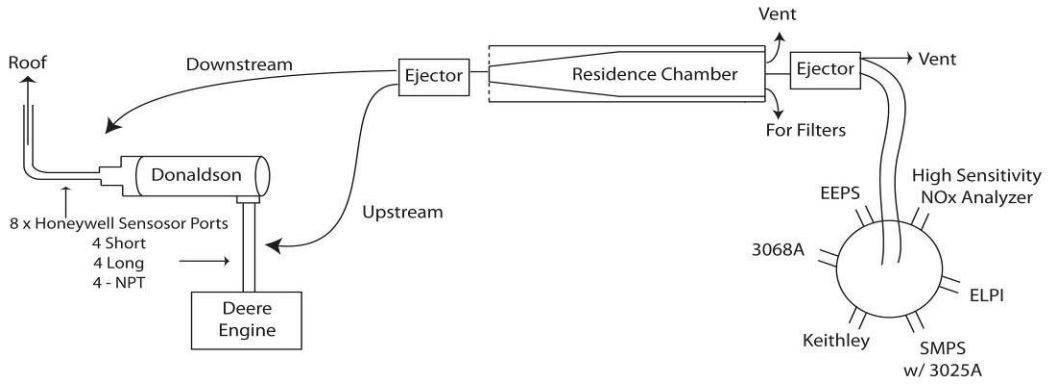

Figure 5. Sampling system schematic

4. Procedure

To ensure day-to-day consistency the aerosol instrumentation was first evaluated using a known aerosol consisting of an atomized solution 100 ppm of dioctyl sebacate (DOS) and isopropyl alcohol. This polydisperse aerosol was then dried using a charcoal diffusion drier and diluted with cleaned compressed air before being distributed to the instruments for comparison. Engine testing was not conducted until all instrumentation showed satisfactory results during this comparison. In some cases this meant rigorous cleaning or replacement of fouled components.

During engine testing a HEPA filter was used at the beginning of each test to ensure the system was leak free. Gas analyzers were zeroed and spanned using NIST traceable gasses at the beginning of each test to insure proper reading and compensate for small day-to-day variations.

Honeywell sensor testing began on the John Deere engine with an initial evaluation of the sensors response over a range of engine speeds. The engine was configured so fueling could be controlled with an analog input. This was achieved using a National Instruments USB-6008 module and LabVIEW software. The software was used to configure the USB module to continuously ramp the engine speed while under constant load. A torque of 250 Nm was chosen because it was the maximum torque which could be achieved at all desired speeds. The engine speed was ramped at a constant rate of 2 RPM per second from 900 to 2400 RPM, the rated engine speed, and then back

to 900 RPM. During the ramp test particle emissions were monitored in near real-time using the sampling system shown in Figure 5 upstream of the Donaldson filter. Emissions were measured using the EEPS, AVL and Honeywell sensor. The instantaneous dilution ratios were determined from raw and dilute NO measurements.

The response of the sensor was then evaluated during a simulated DPF failure using a valve which allowed a portion of the exhaust to bypass the filter. Given the limitation of the number of DPFs available for testing it was desirable to try and simulate a DPF failure without immediately breaking a DPF, thus tests were conducted using an exhaust bypass pipe with an inner diameter of 4.1 cm (1.61 in) and gate valve to simulate a "leaking filter". It was hoped that this simulation would enable a better calculation of how many holes or how much DPF surface area needed to be broken before failure would occur. In this case failure is defined as exceeding the on-road standard of 13 mg/kWh (10 mg/bhp-hr) downstream of the filter. Testing began with a 15 min warm-up to bring up engine temperatures followed by 15 min at high load to regenerate the Donaldson DPF. After warm-up the engine was adjusted to the test condition and allowed to stabilize for another 30 min before sampling began. Stabilization time was determined by continuously monitoring EEPS, AVL and NO concentrations as well as all temperatures and pressures. Once all values had reached steady state sampling began.

After the simulated failure the bypass valve was removed and the DPF was actually failed in a series of steps by drilling holes in the DPF end-caps. In addition to the instrumentation used during the simulated failure, gravimetric filter samples were collected during the actual failure of the trap. Gravimetric filter samples were collected on 47 mm Teflon filters at a flow rate of 72 L/min. Filters were weighed using a Cahn Microbalance and values reported are the averages and standard deviations of 4 filters.

Due to an unexpected dynamometer failure, testing moved to the Isuzu engine during the DPF failure tests. During the switch to the Isuzu engine, a suitable condition was selected which gave soot concentrations, flows, and temperatures, similar to the John Deere engine. The Isuzu engine is a more modern on-road engine which had lower engine out particle emissions than the Deere at a similar engine condition. To better

simulate the emissions from the Deere engine the intake air flow was throttled (restricted) causing the engine to run closer to stoichiometric conditions resulting in increased PM emissions. The throttle was adjusted so the AVL measurement upstream of the filter was similar to what was seen on the John Deere engine before the dynamometer failure (~14 mg/m^3).

After failing the DPF a final series of experiments were conducted, that looked more closely at the charge state of particles before and after the failed DPF. An identical Donaldson catalyzed filter (part # 226355-016-190; 26.7 x 35.6 cm) was available for use from a previous project. This filter had not been failed and was used so the bypass valve conditions could be repeated with an unmodified filter. A homebuilt DMA similar in design to that described by TSI was used with the ability to switch voltage polarity. Located downstream of the DMA was a CPC and an electrometer. This allowed for the simultaneous measurement of particle concentration and net electrical charge, as well as the calculation of average charge per particle as a function of electrical mobility.

5. Results and discussion

5.1 Sensor response to transient engine speed

Results of the engine speed ramp test are summarized in Figure 6. The notation "UP" and "DOWN" corresponds to the increasing speed ramp and decreasing speed ramp. These data are plotted together against engine speed. The EEPS and AVL are in good agreement, regardless of whether the engine speed is increasing or decreasing, and show a clear trend. However, the Honeywell sensor shows a repeatable trend that does not appear to track with the other instruments.

Data from the Honeywell sensor were collected using an improvised system built by the University. The reason these data were collected was so that the raw, untreated signal from the Honeywell sensor could be observed without using Honeywell proprietary data acquisition hardware and software. Data were collected using a Kistler charge amplifier and analyzed by calculating the root mean square (RMS) voltage of the

output. As mentioned earlier, it is important to note that this is not the same charge amplifier which is imbedded in the Honeywell electronics but rather an independent test, which was conducted by the University of Minnesota to look at the raw response of the sensor to changing engine speed without any Honeywell proprietary filtering.

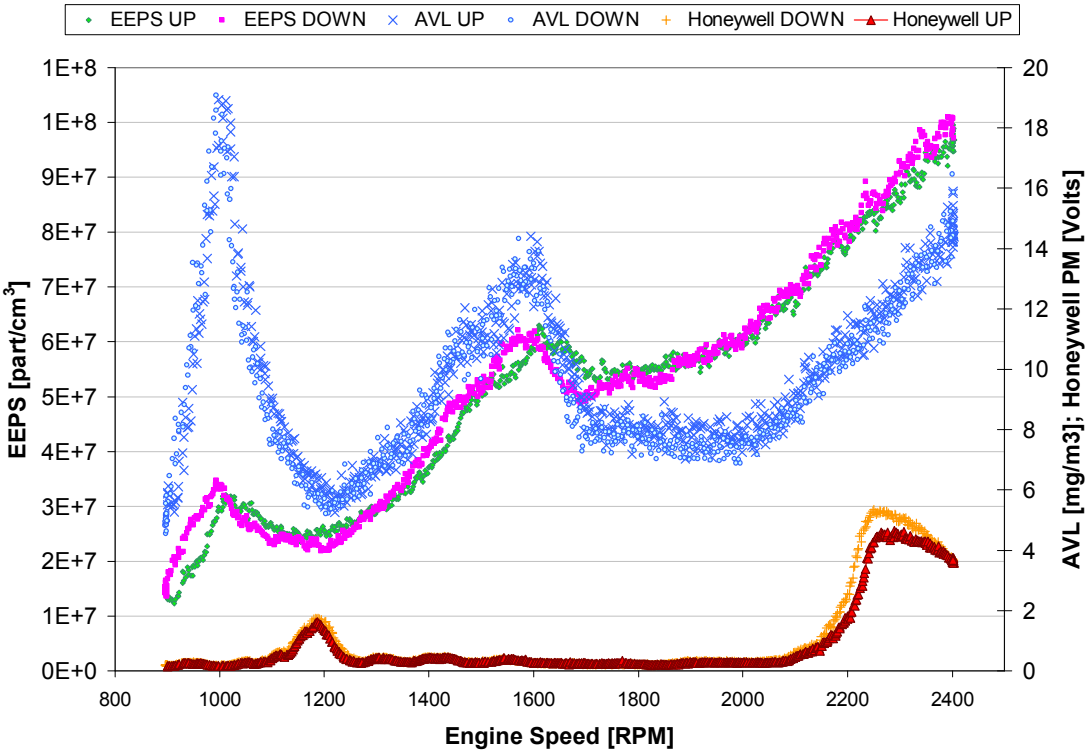

Figure 6. EEPS, AVL and Honeywell PM sensor response during engine speed ramp conducted at constant 250 N-m torque engine out measurement without DPF

Throughout the engine speed range there are a number of peaks and valleys which were observed by the EEPS and AVL indicating high or low concentrations in particle mass or number concentration. Though these features roughly line up, the ratio of EEPS number concentration to AVL mass concentration varies. At 1000 RPM the measured EEPS size distribution has a large accumulation mode with a mean size just above 70 nm. At speeds above 2000 RPM the particles are smaller and mean particle diameter has shifted closer to 50 nm. This results in a larger number to volume ratio, N/V, for higher engine speeds and a lower N/V at 1000 RPM, with 250 Nm of torque. Particle length (d1)

and surface area (d2) will have weightings which fall between particle number (d0) and particle volume (d3).

The unfiltered Honeywell sensor response with a Kistler charge amplifier does not appear to track with either of the particle instruments. The source of the signal shown in Figure 6 was unknown but mechanical vibration was suspected. To further investigate this assumption an accelerometer was added to the exhaust system to measure vibration. The accelerometer was in the same orientation as the Honeywell sensor, but located one exhaust port, 5 cm (2 in) downstream of the Honeywell sensor.

5.2 Vibration testing

Tests with the accelerometer and Honeywell sensor with Kistler charge amp were conducted for a number of load and speed combinations giving similar results. Figure 7 shows one such case. Data were logged for both sensors at 2 kHz and a fast Fourier transformation (Cooley and Turkey, 1965) was used to convert these data to the frequency domain.

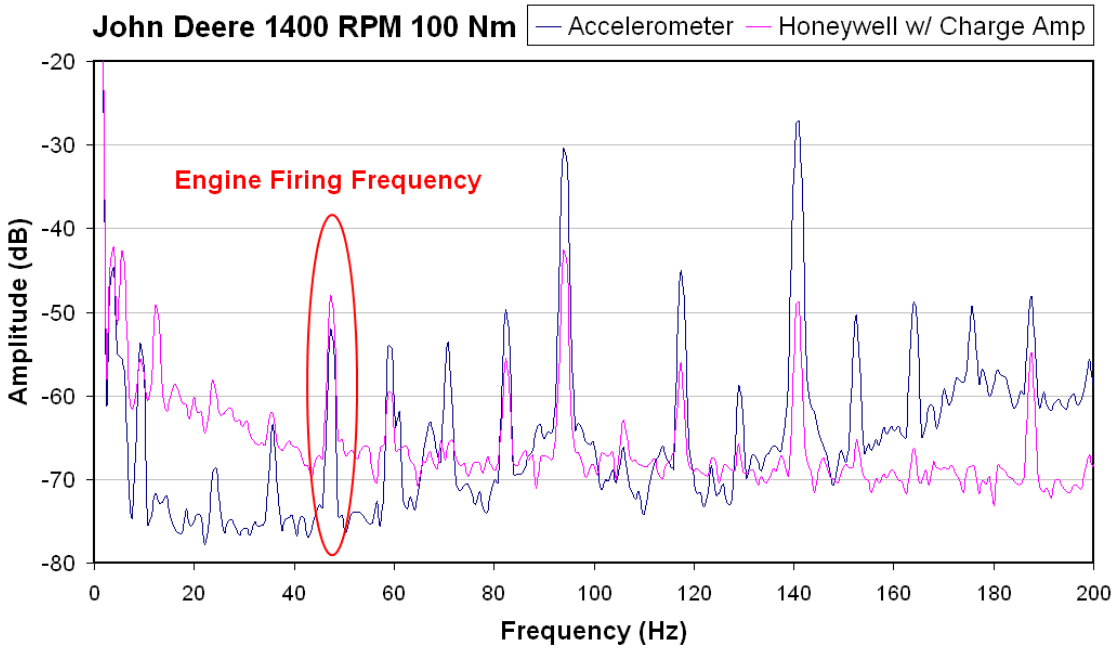

Figure 7. Accelerometer and Honeywell sensor response at 1400 RPM and 50 Nm

The John Deere engine has 4 cylinders and was rotating at 1400 RPM so an exhaust event occurred at a rate of 46.7 Hz. This peak is clearly visible as a component of the response from both sensors. Thus interference from mechanical vibration apparently is masking the signal which is expected from each individual exhaust event. In an attempt to remove the vibrational components of the signal another test was conducted where the sensor was held in the exhaust without touching the exhaust pipe. This created a small exhaust leak at the port where the sensor usually was screwed into the exhaust pipe, but backpressure from the exhaust system kept the flow of exhaust outward and over the sensor. Figure 8 shows the response of the Honeywell sensor suspended in the exhaust stream and then screwed into the exhaust bung making the usual rigid mechanical connection. Data were collected using a Kistler charge amplifier and logging of the output was triggered by an encoder on the engine which gave a pulse every 0.5 crank angle degree.

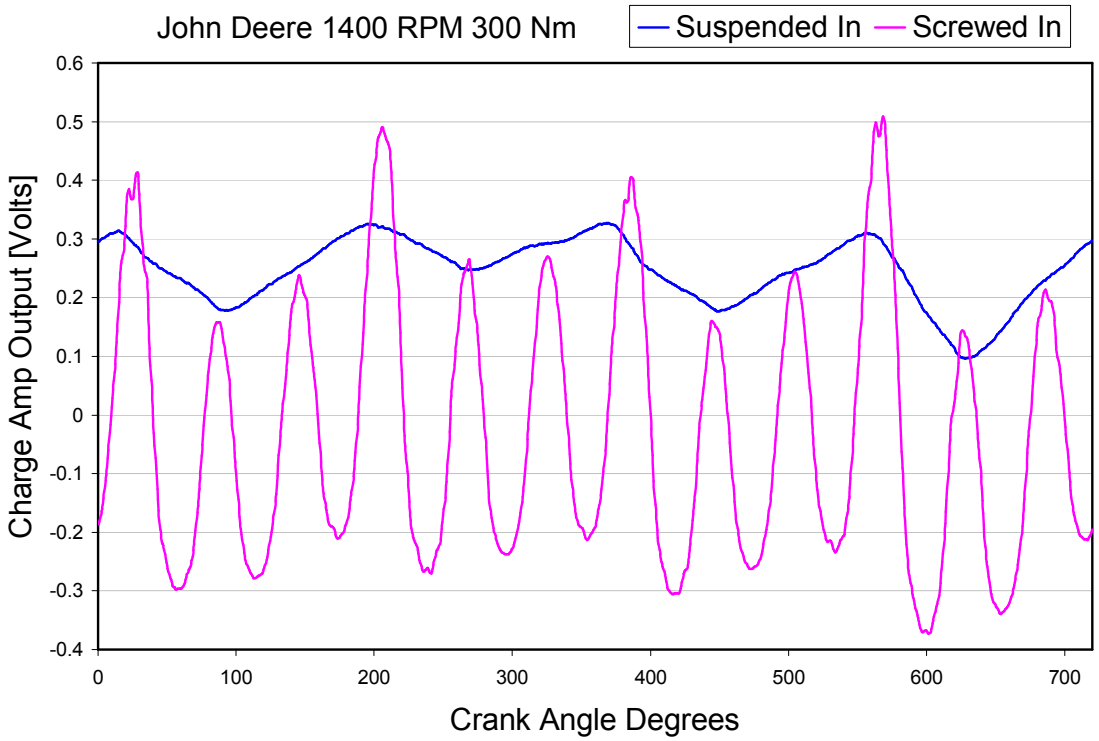

Figure 8. Honeywell sensor suspended in exhaust

Data are shown in Figure 8 for 720 crank angle degrees, one engine cycle. During this engine cycle four exhaust events occur, one for each cylinder. When the sensor was not rigidly connected to the exhaust pipe exhaust events are clearly visible. However, once the sensor was connected this signal was masked by a much larger, seemingly sinusoidal signal assumed to be vibrational noise. Removal of the vibrational component of the signal can either be done through signal processing or redesigning the sensor and mount to reduce the response to mechanical vibration.

5.3 Simulated failure of the DPF

With the DPF and bypass valve installed upstream emissions were monitored as the valve was opened to determine the effects on upstream emissions. It was expected that opening the bypass would cause a decrease in engine back pressure which could change engine out emissions, but in fact the valve had a negligible effect on upstream emissions even though it had a considerable effect on engine backpressure. Instruments were then moved downstream of the DPF and data were collect with the bypass valve at 0%, 25%, 50% and 100% open.

5.3.1 Effects of engine backpressure

The 4.5 L John Deere 4045 engine was used for backpressure testing. The engine was operated at 2400 RPM and 100 N-m. Exhaust pressure and temperature were measured after the engine turbo. The dilution system has been described above. The bypass was a pipe and gate valve with an internal diameter of 4.1 cm (1.61 in). Percent open was determined as the number of turns divided by the total number of turns from fully closed to fully open. Figure 9 shows the sampling configuration and bypass location.

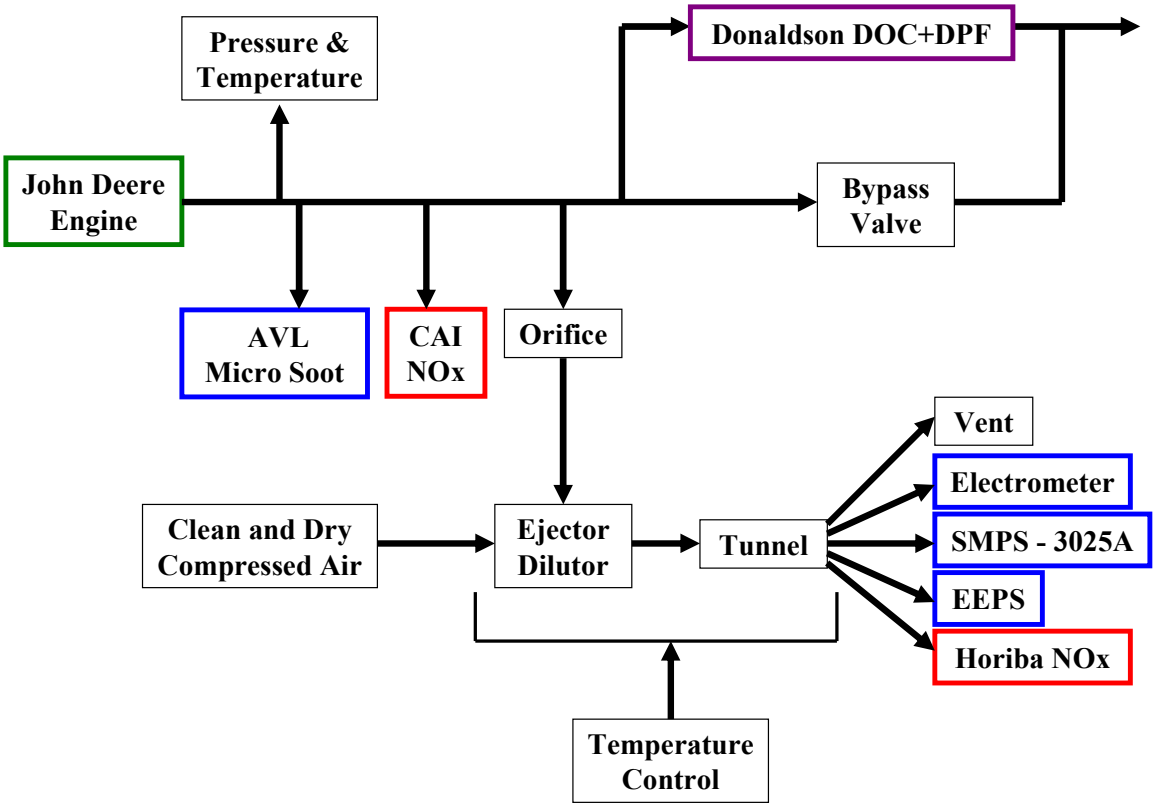

Figure 9. Backpressure testing schematic

After determining changes in backpressure due to the bypass valve had a negligible effect on upstream emissions, the instrumentation was moved downstream of the Donaldson DPF. Figure 10 shows the configuration of the instrumentation for sampling downstream of the DPF while the bypass valve is adjusted.

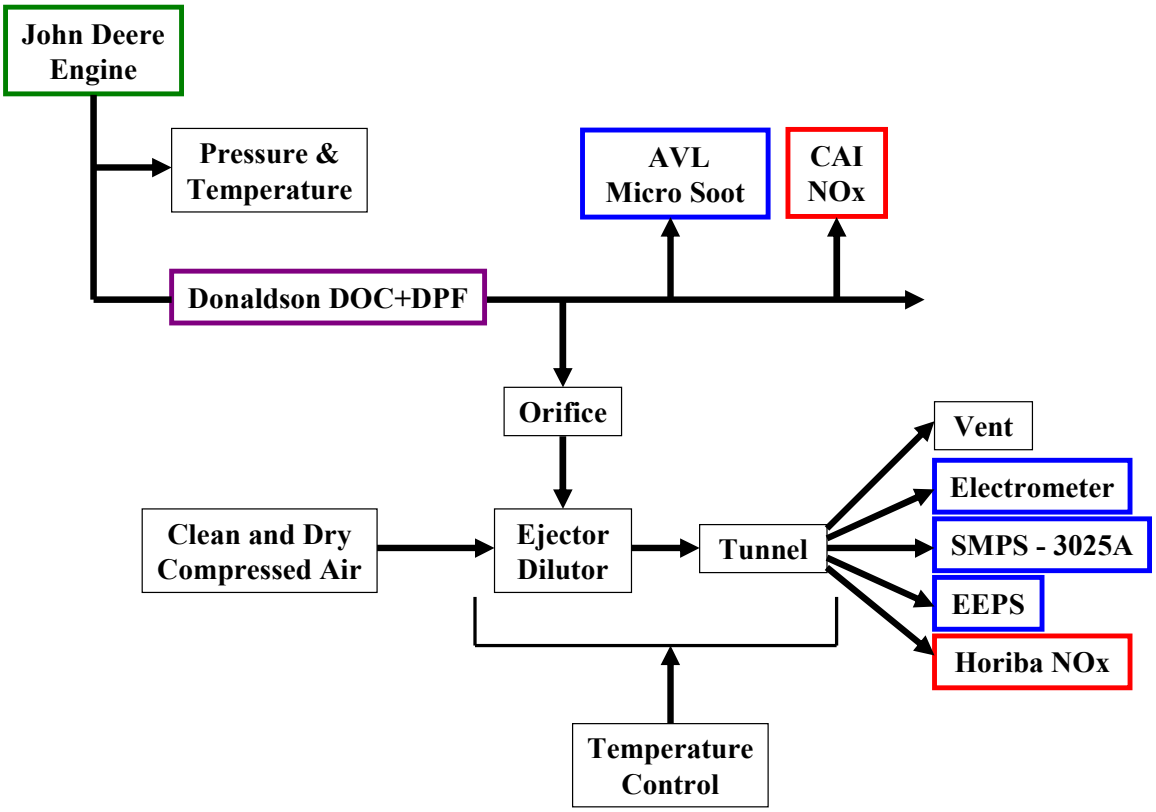

Figure 10. Instrument configuration for downstream sampling

5.3.2 Bypass valve results

Figure 11 shows the SMPS and EEPS number weighted size distributions for the different valve positions with standard deviations. The engine is operating at 1400 RPM and 350 Nm of torque which is a mid-load condition. As expected the concentration of the accumulation mode particles increased with increased valve open position, i.e. larger leak. At the tail of the accumulation mode the EEPS drops off more rapidly than the SMPS. This phenomenon occurs because agglomerates pickup more charge in the charging section of the EEPS then a comparably sized spherical particle and the EEPS data inversion is currently based on spherical particles. This gives the particle a higher electrical mobility which causes it to be classified as a smaller size. This results in the EEPS size distribute dropping off faster than the SMPS as well as a high peak concentration due to the overly charged particles registering in a smaller size bin. This

has been observed previously (Wang et al., 2009) and TSI is working on a modification to the EEPS algorithm to correct this problem.

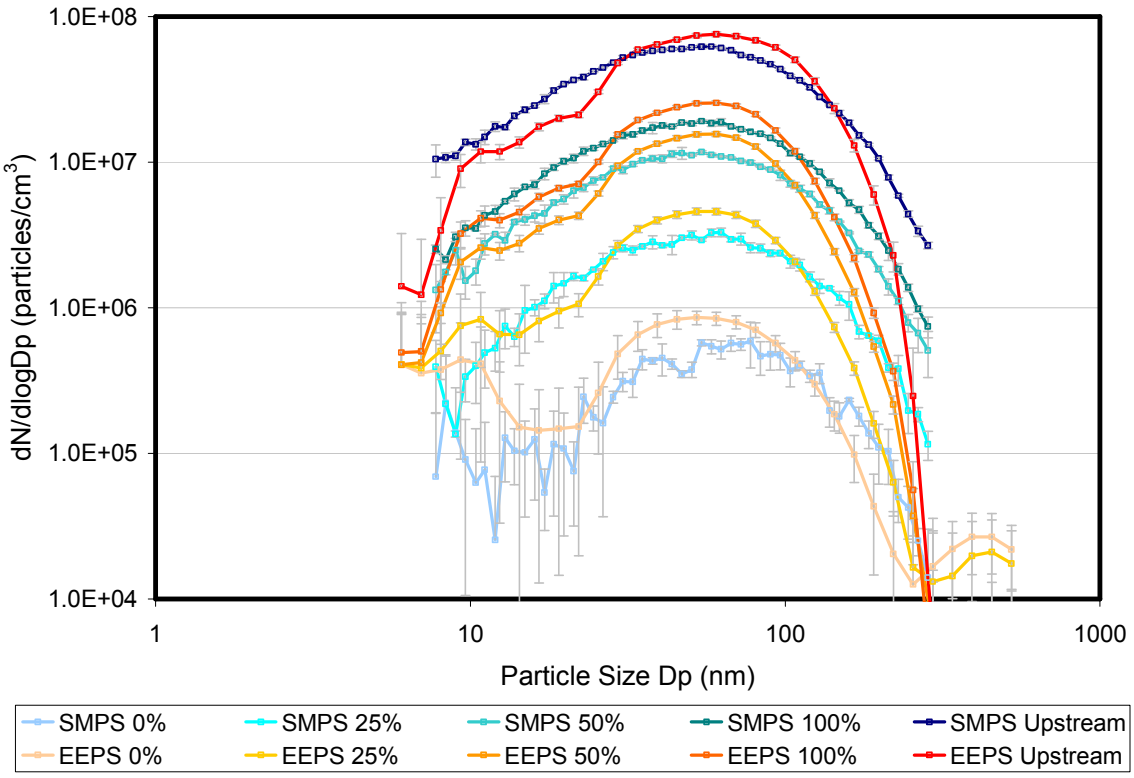

Figure 11. Size distributions for varying levels of bypass valve opening

As the bypass valve is closed the shape of the size distribution remains essentially the same but the magnitude is reduced as expected. The only exception to this interpretation occurs when the valve is "fully closed," 0% open. In this position the majority of PM is coming through the trap rather than the valve and there appears to be a small nucleation mode tail around 10 nm. This is likely due to nucleation of volatile materials that are adsorbed on existing accumulation mode soot particles when more soot is present.

Figure 12 and Figure 13 show mass concentration and brake specific mass concentration as measured by the AVL and calculated from the EEPS and SMPS data. As expected, concentrations decrease as the valve is closed. SMPS mass concentrations were

derived from the size distribution and an assumed density of 1g/cm^3 for particles less than 50 nm and a density of (50/Dp)^(0.6) for particles larger than 50 nm. This density and size relationship has been reported previously (Park et al., 2003). EEPS mass concentrations were determined assuming a constant density of 1g/cm^3 because of the misclassification of particles due to over charging of large agglomerates, discussed earlier, the particle density and size relationship is not as simple. In Figure 12 and Figure 13 the SMPS and EEPS track the AVL measurements but there are significant differences in the average concentrations. The cause of these differences is believed to be each instrument uses different assumptions and algorithms to estimate mass concentration.

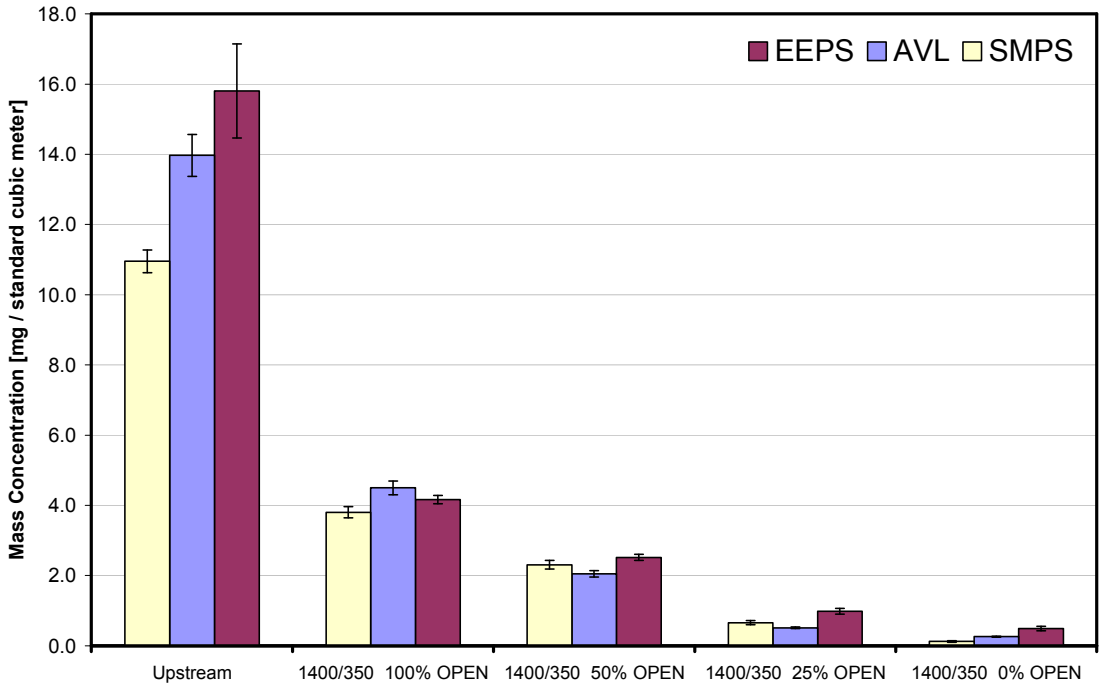

Figure 12. Mass concentration with varying amounts of valve opening

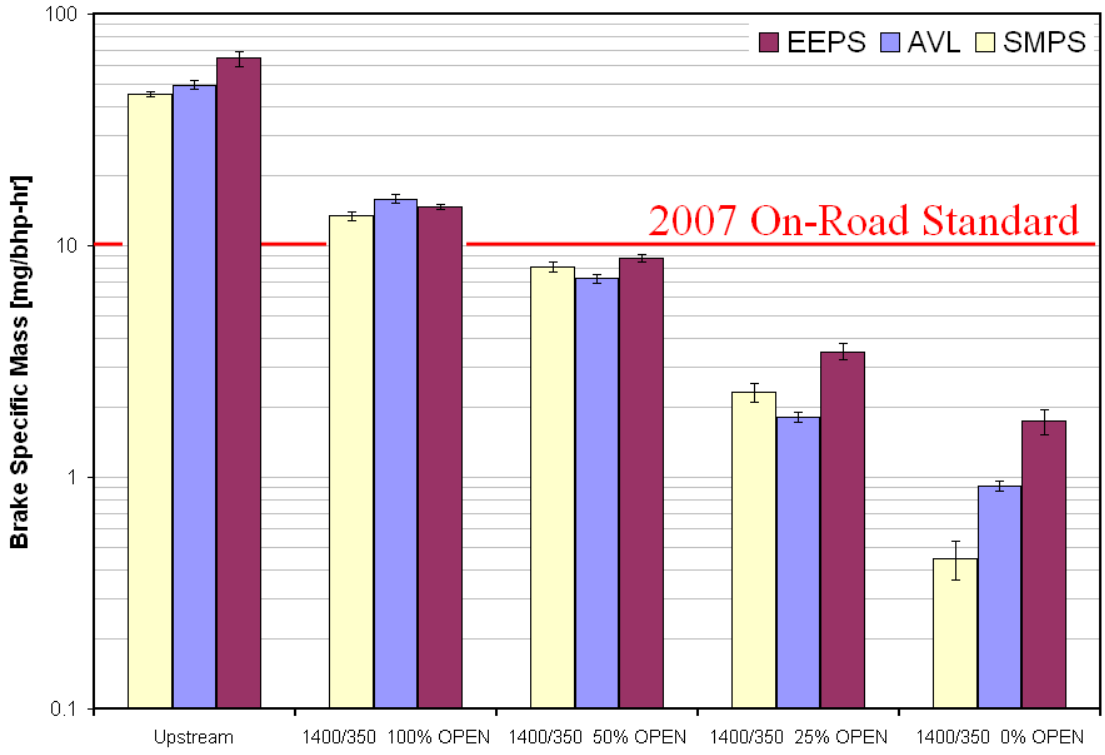

Figure 13. Brake specific mass emissions for varying amounts of valve opening

Figure 14 shows the AVL brake specific mass emissions from Figure 13 and Honeywell sensor signals for varying amounts of bypass valve opening. The four Honeywell sensors have different responses but the general trend shows increasing response with increasing soot concentration for any given probe. This indicates probe placement may have a strong effect on the magnitude of the sensor response. Individual probes may also respond differently when exposed to the same soot concentration.

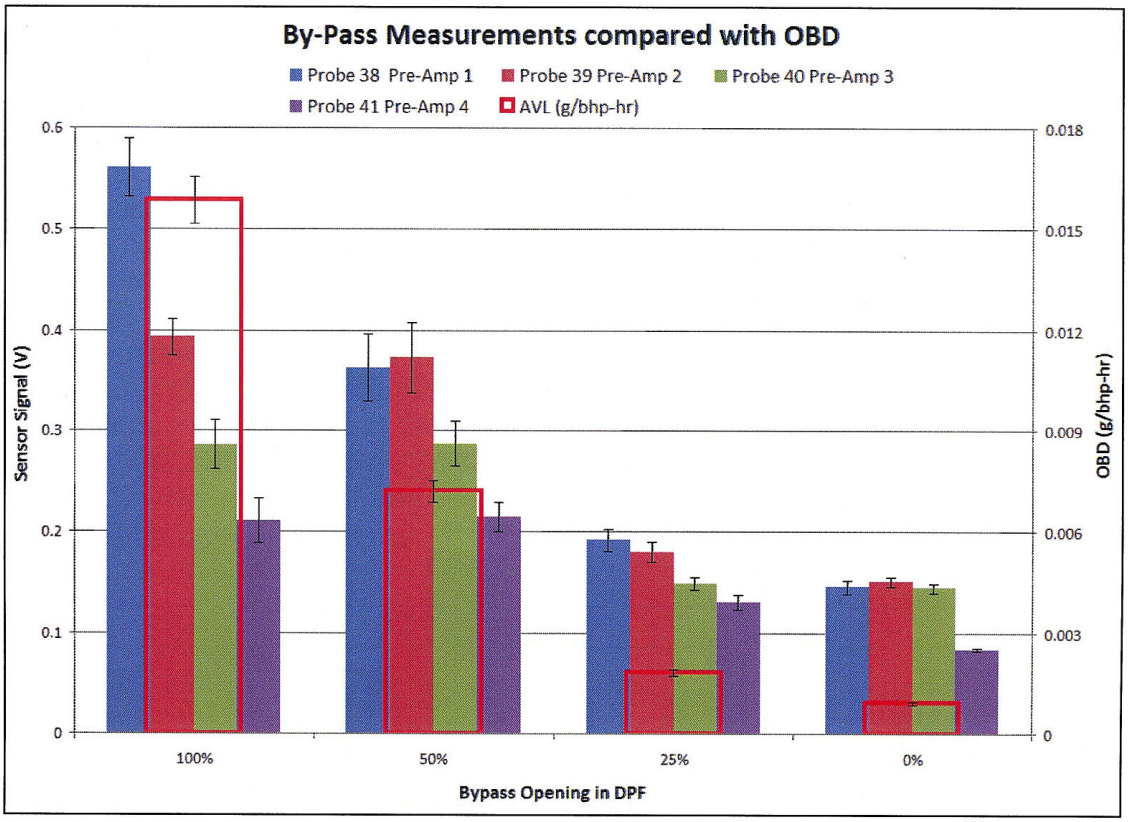

Figure 14. Honeywell sensor signal for varying amounts of valve opening

5.4 Failing the Donaldson DPF

Donaldson DPF failure was simulated by first drilling a series of holes and later by milling out one large section. The reason for this was that estimating failure by the number of holes drilled out did not yield the expected degree of failure. Even when many channels were drilled out the DPF still had a higher degree of removal efficiency than would be expected from the exposed cross-sectional area compared to that of the bypass. This is because the pressure drop along a long narrow DPF channel is significant enough to still promote wall flow even with the end drilled out. Therefore it was decided to mill a large area of the end caps. Pictures of this process can be found in Appendix C. After each level of failure the filter was reinstalled and PM emissions downstream of the DPF were evaluated. These results were then compared to testing conducted with the exhaust bypass valve.

5.4.1 Failing the DPF

A cutaway showing the internal flow path through a section of the Donaldson DPF is shown below in Figure 15. The DPF has 100 cells per square inch (15.5 cells/cm^2) with a 0.43 mm (0.017 in) wall thickness. Therefore, the open area of any given cell is a square with a side length of 2.1 mm (0.083 in). Each cell is 35.6 cm (14 in) long.

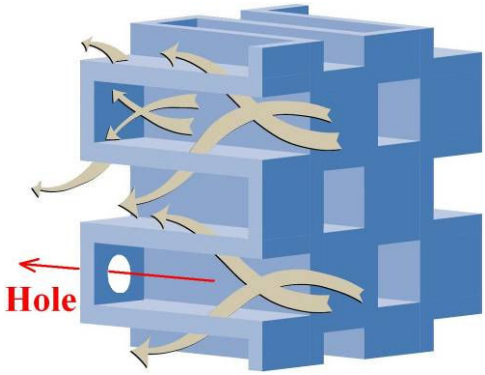

Figure 15. Flow path in Donaldson DPF

Source: (Donaldson, 2008) as modified by Ragatz

The DPF was failed by drilling out end caps on the outlet side of the filter. This allows some of the exhaust to enter the filter through an open channel and exit the filter through a hole in the end cap on the opposite end. A sufficiently small, 0.0625 in drill bit was chosen to fail the end caps in order to minimize damage to the filter wall. The holes were drilled by hand using a cordless drill. This process is shown in Appendix C. Failure started in the center and then moved outward. Appendix C shows the hole patterns which were drilled. Emission testing downstream of the Donaldson DPF was conducted with 0, 100, 200, 300, 600, and 900 holes. For the final failure it was decided that 1800 end caps (42%) would be milled off which included all end caps which originally had holes.

5.4.2 Setup for testing of the failed DPF

PM emissions testing downstream of the failed DPF was conducted in the same manner as testing done downstream of the filter and bypass valve. The sampling system is shown in Figure 10. However, testing began on the John Deere engine but was subsequently moved to the Isuzu engine due to a malfunction within the John Deere

dynamometer which rendered it inoperable. Conditions of 0, 100, 200, 300, and 600 drilled holes were tested with the John Deere engine, while 900 holes and 1800 milled end caps had to be tested with the Isuzu engine. PM emissions were monitored using the SMPS, AVL, EEPS, and gravimetric filters. SMPS and EEPS mass concentrations were derived as discussed previously.

5.4.3 Results of DPF failure

Discrepancy between 0% valve opening and 0 holes is attributed to valve leakage. The gate valve had a metal on metal seal to tolerate the extreme temperatures in the exhaust, but this type of seal is prone to leakage. The bypass valve was removed during the DPF failure tests to ensure no exhaust could leak around the valve. The base case for the unmodified filter (0 Holes) with the bypass removed showed greater than 99% removal by mass and number.

The DPF was then failed until the 2007 on-road standard was exceeded. Milled 1 and 2 correspond to two different levels of engine throttling, i.e., upstream concentration with the same number of holes. The same particulate levels as 100% valve opening were not reached until 1800 end caps were milled off of the filter. This corresponded to an open area of 12.4 in^2 (80 cm^2). The cross section of the valve at 100% opening only has an open area of 1.77 in^2 (11.4 cm^2). This is partially because the exhaust flow going through the failed DPF has gone through a diesel oxidation catalyst (DOC) which is upstream of the filter, and flow going through the bypass valve does not. The DOC will remove a portion of the volatile hydrocarbons in the exhaust stream, but leave the elemental carbon mostly unaffected. However, a major contributor to this discrepancy is that the open area of the failed filter is made up of a large number of narrow long channels. Even though the failed channels are open on both ends they still promote wall flow by having a relatively large pressure drop due to their geometry. Figure 16 shows brake specific mass concentrations downstream of the filter.

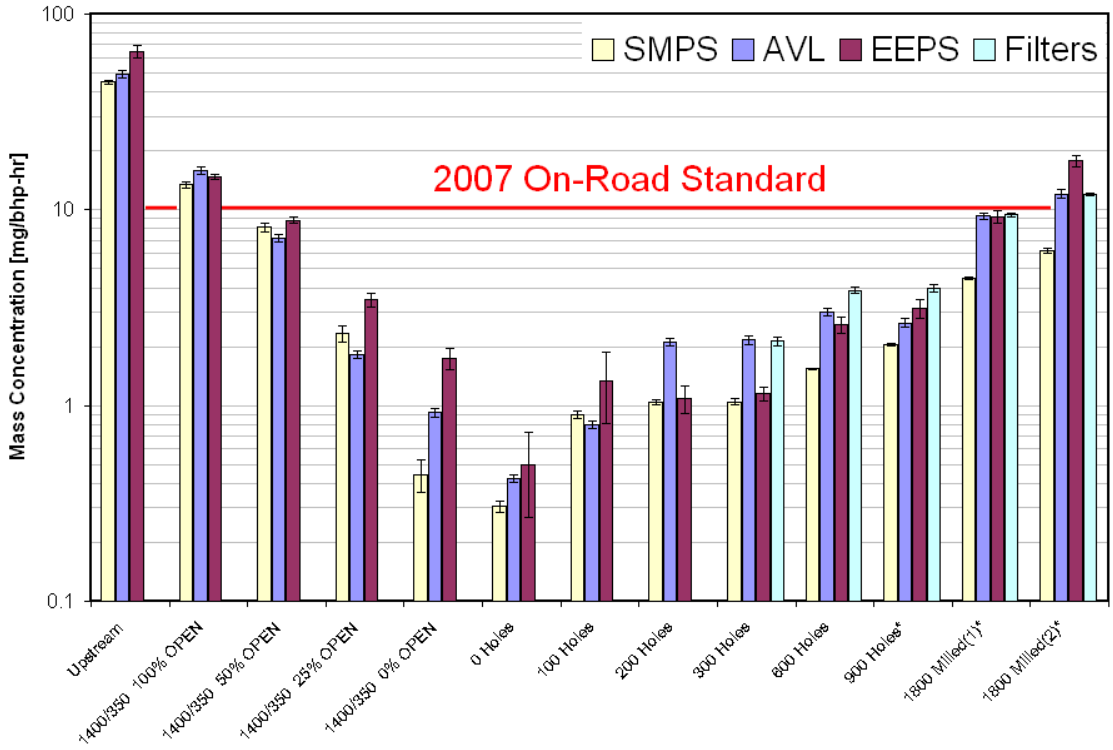

Figure 16. Brake specific mass concentration

The current PM mass emission standard for an on-road heavy-duty diesel engine is 10 mg/bhp-hr. This threshold is crossed between 50% and 100% valve opening and 1800 milled holes from throttling position 1 to 2. For the failed trap the AVL and gravimetric filter samples are considered the standard and show excellent agreement.

Figure 17 shows the response of the Honeywell sensor during the simulated and actual failure of the DPF. There is a clear difference in the response of the sensor for a failed trap verses the bypass at a similar soot concentration. The sensor also has a drastically different response on the Isuzu engine. This is most likely due to the differences in the exhaust system when switching engines. After the failure of the John Deere engine's dynamometer, the Donaldson DPF was kept in place and the Isuzu exhaust was routed to its location. This long transfer line acted as a vibrational damper. The Honeywell sensor is prone to interference from mechanical vibration which may explain the drastic decrease in magnitude when switching engines.

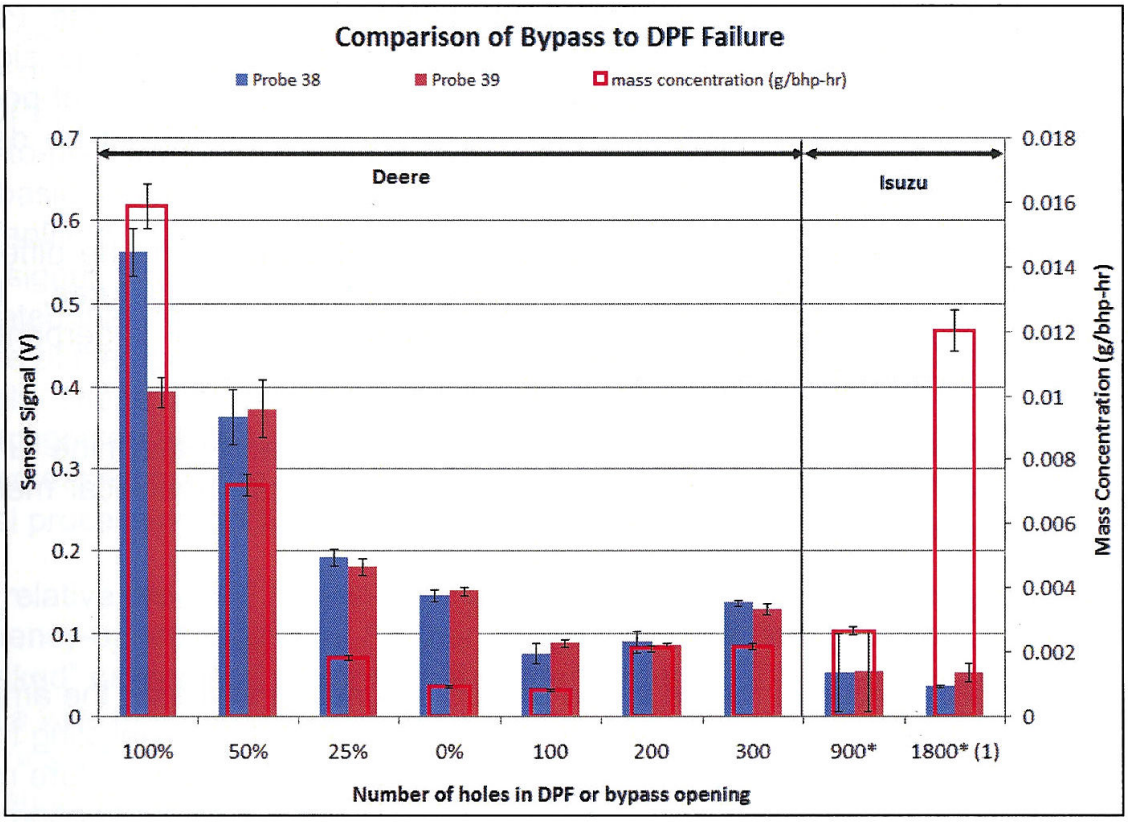

Figure 17. Honeywell sensor response during DPF failure

5.5 Charge measurements

During the failure of the DPF charge measurements were made to better understand the nature of the particles penetrating through the failed trap. Figure 18 shows the measured charged fraction and Boltzmann equilibrium for a number of conditions. This measurement was made by putting an electrostatic precipitator before the SMPS. Three scans were taken with the voltage off and then the voltage was turned on to 7 kV, removing all charged particles and allowing only the neutral particles to pass through. An additional three scans were taken and by subtraction the fraction of particles carrying a charge can be found. The electrostatic precipitator removes charged particles regardless of polarity. The center rod is held at +7 kV and the outside is grounded so positively charged particles are lost to the outside wall and negatively charged particles are lost to the center rod. This measurement becomes increasingly difficult at low concentrations,

and is the reason for large error bars on the 300 holes case. For all other cases shown the charged fraction falls between Boltzmann equilibrium at 1000 Kelvin and 1500 K.

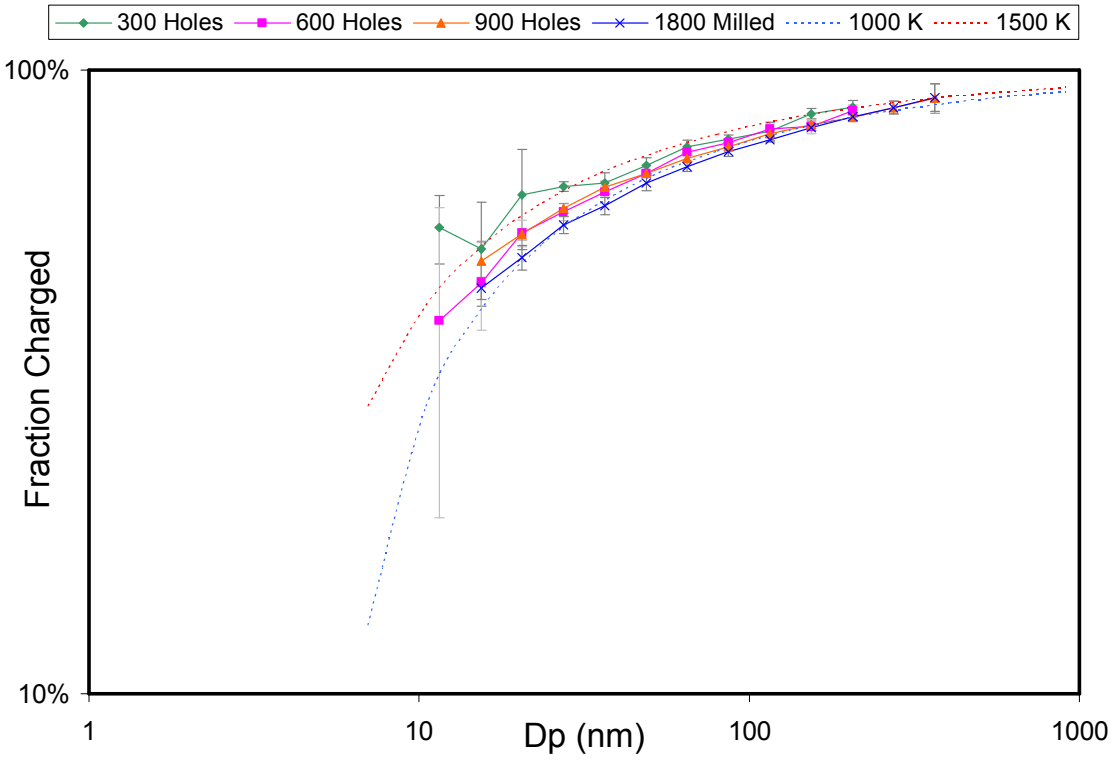

Figure 18. Charged fraction

Figure 19 shows the net charge of the aerosol sample after dilution. A near zero net charge means the number of positive charges and negative charges are balanced. A positive value in Figure 19 indicates a higher number of positively charged particles. An aerosol can have a high charged fraction and still be net neutral. Figure 18 and Figure 19 show that as the filter was being failed the fraction of particles caring some degree of charge stayed relatively constant but the net charge increased.

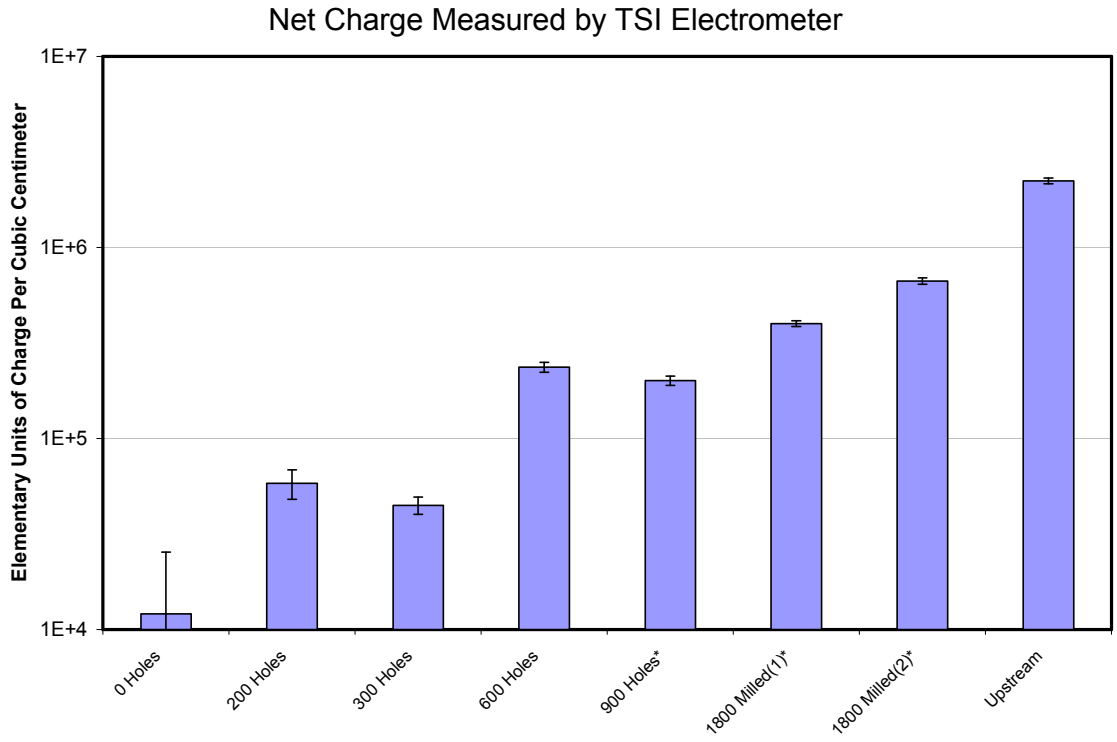

Figure 19. Net charge

Figure 20 shows a cross plot of net charge penetration through the filter as it was failed and AVL mass normalized to upstream concentrations. They were found to have a linear correlation coefficient of R^2=0.993 and slope of 0.998. This suggests the measured net charge is proportional to the mass penetrating through the filter.

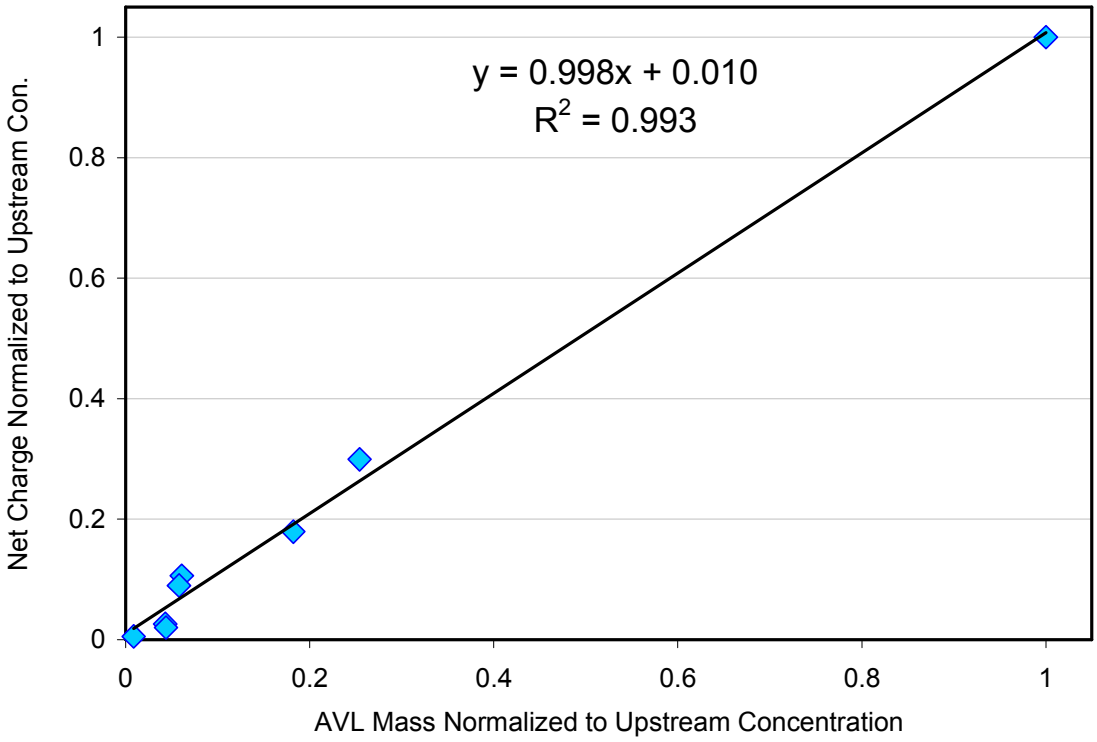

Figure 20. Net charge vs. AVL mass normalized to upstream concentrations

5.6 A closer look at charge

In the previous section an electrostatic precipitator has been used to determine the fraction of particles caring a charge and an electrometer has been used to determine the overall imbalance in charge or net charge. The sampling system in Figure 21 uses a DMA to separate particles by polarity and classify them by electrical mobility. The monodisperse aerosol then goes to a CPC and the electrometer simultaneously. The voltage on the DMA is ramped exponentially from 10 to 10,000 volts over a 2 min period and then back. This results in a mirror image about a central point which can be used to determine, and correct for the delay time to each instrument. Measurements were made with and without a neutralizer and with positive and negative polarity on the DMA.

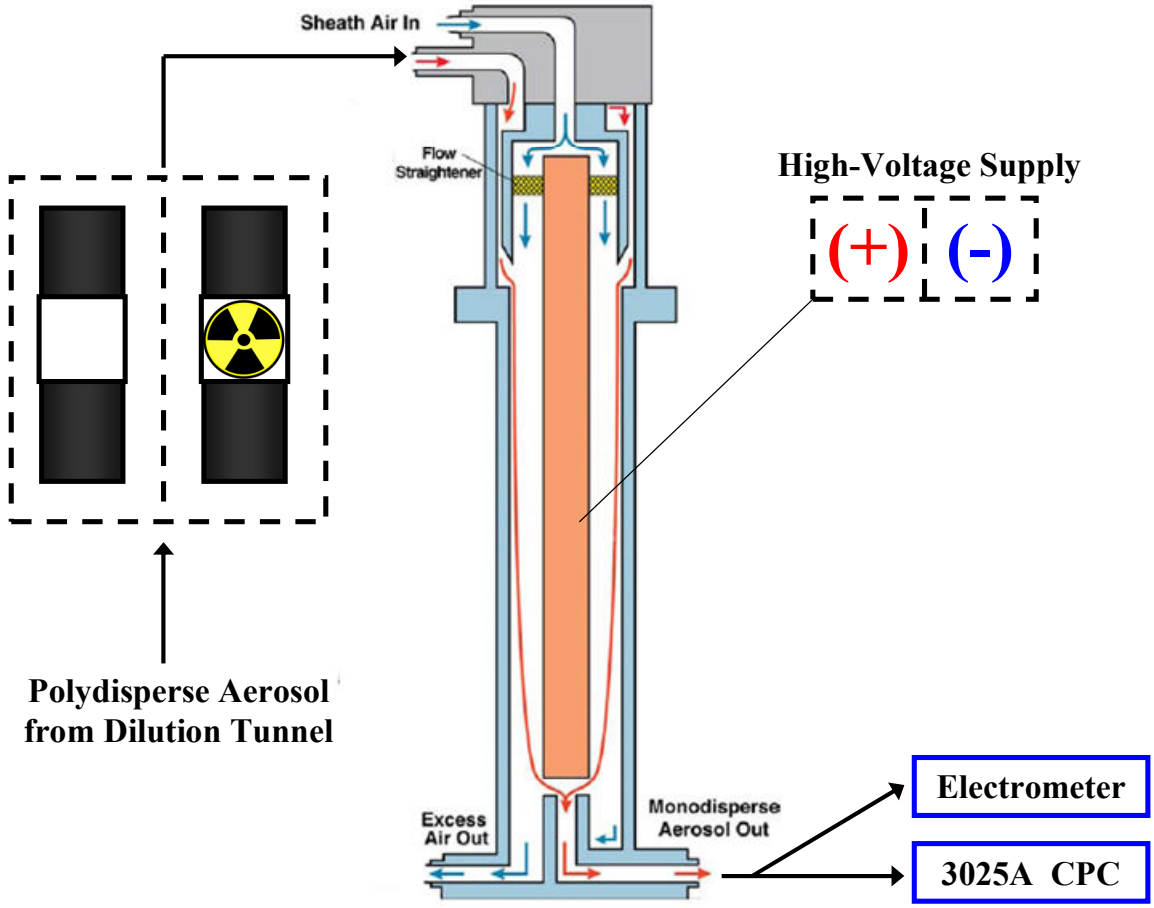

Figure 21. Charge measurement sampling schematic

Source: TSI as modified by Ragatz

This system was first used to evaluate a DOS aerosol distribution and then used to evaluate dilute diesel exhaust from a 4.5 L John Deere engine operating at 1400 RPM and 350 Nm of torque, with no aftertreatment. Figure 22 shows the CPC and electrometer outputs as the voltage was ramped from 10 V to 10,000 V and back to 10 V over a four minute sample period. The readings are corrected for delay time using the symmetry of the up and down scans. The notation "NO" and "YES" indicates whether a neutralizer was used during sampling. "POS" and "NEG" indicate positive and negative column voltage respectively. A positive voltage on the center column of the DMA will attract negatively charged particles and produce a negatively charged monodisperse aerosol, resulting in a negative reading from the electrometer.

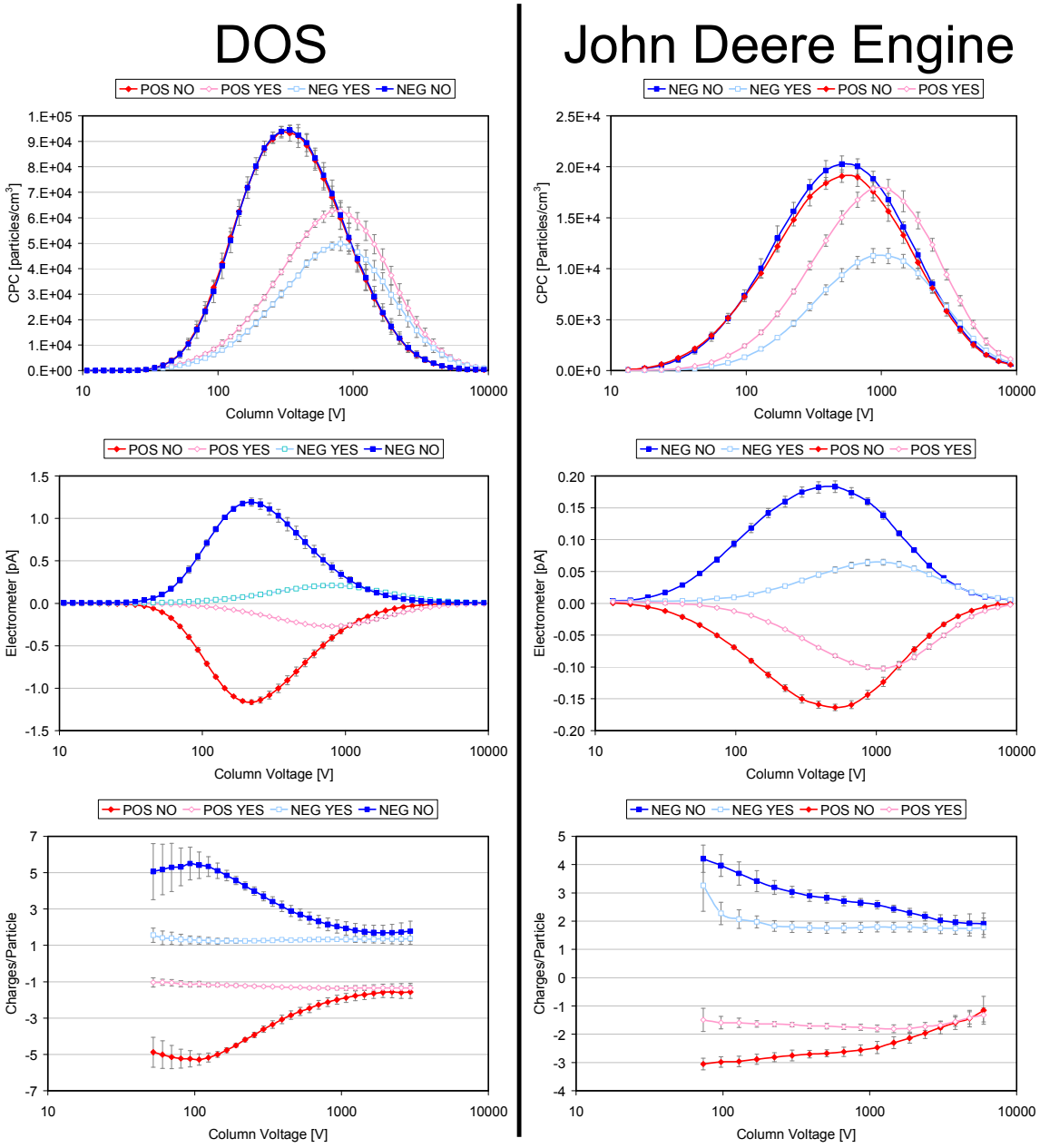

Figure 22. Measurement of charge per particle using DOS and engine exhaust

When using the neutralizer, the CPC shows a higher peak concentration for negatively charged particles (positive column voltage) in both cases. This is attributed to the difference in mobility for positive and negative ions. The DOS distribution shows a difference of ~20% in peak CPC concentration which is expected for spherical particles

(Gunn, 1956; Wiedensohler and Fissan, 1988). However, the difference is much greater for engine exhaust from the John Deere ~60%. This difference is attributed to the morphology of the diesel exhaust particles. Studies have shown that agglomerates can have a higher charging efficiency than spheres (Lall and Friedlander, 2006; Wang et al., 2010).

When switching from using a neutralizer to using no neutralizer the peak of the CPC distribution shifts to a smaller voltage. This is expected since the untreated aerosol from engine exhaust and the nebulizer will have a higher charged fraction and greater incidence of multiply charged particles, representative of a high temperature Boltzmann distribution. Once the aerosol passes through a neutralizer some of the multiply charged particles will become singly charged with a lower electrical mobility, therefore registering at a higher voltage. The neutralize will also increase the fraction of neutral particles if the incoming distribution is representative of a high temperature Boltzmann, thus decreasing the magnitude.

The particle concentration and electrometer current can be used to determine the average charge per particle as a function of electrical mobility. While using the neutralizer the spherical DOS particles are mostly singly charged, if they are carrying a charge at all, with an occasional multiply charged particle making the average just larger than one across the entire mobility range. For dilute exhaust the average charge per particle is much closer to two. This is attributed to particle morphology showing agglomerates can have a higher charging efficiency than spheres (Lall and Friedlander, 2006; Wang et al., 2010).

Appendix D shows the distributions from Figure 22 plotted against singly charged equivalent particle size as well as results from the Isuzu engine with no aftertreatment, bypass valve, and failed DPF. Results from the Isuzu testing show similar trends as the comparison of DOS and exhaust from the John Deere engine. The trends discussed above hold true for raw exhaust, bypass valve, and the failed DPF. The charge state of the aerosol does not appear to be changing significantly as it passes through the failed DPF. This result is important because it shows that though there were some issues with this

particular charge based soot sensor in this study, the concept should still work if appropriate actions were taken to isolate the charge signal from the exhaust.

6. Conclusion

Engine exhaust from a diesel engine was characterized using an AVL micro soot sensor and gravimetric filter samples for mass measurements, TSI sizing and counting instrumentation for size distributions, and an electrometer and electrostatic precipitator for charge measurements. Measurements were made upstream and downstream of a DPF. The failure of the filter was simulated using a bypass valve and then the filter was actually failed in a series of steps by drilling holes in individual channel end caps. These measurements were used to evaluate a real-time diesel exhaust soot sensor provided by Honeywell. The sensor response was found to be susceptible to error from mechanical vibration. However, when appropriate action was taken to remove the vibrational component, the sensor was able to resolve charge pulses from individual cylinders on a cycle by cycle basis. Honeywell used proprietary algorithms in the post processing of their sensor data in hopes of digitally filtering out vibrational components. If this technique could be further refined such a sensor could have many uses as an engine diagnostic tool. Under steady state operating conditions a signal increase was observed as the DPF was failed but this response was engine and exhaust system dependent.

Further investigation of the engine exhaust charge distribution indicated charge penetration is still a valuable method for determining DPF failure. The charge state of the aerosol does not appear to be changing through the device and the measured net charge tracked well with PM output. However, further work must be done to develop a sensor with the sensitivity to measure these small fluctuations of charge and still have the robustness to handle the harsh exhaust environment and mechanical vibration from the engine.

References

Abdul-Khalek, I., D.B. Kittelson, & F. Brear. "The Influence of Dilution Conditions on Diesel Exhaust Particle Size Distribution Measurements." *Society of Automotive Engineers,* 1999-01-1142 (1999).

Adams K.M., Cavataio J.V., Sale T., Rimkus W.A., Hammerie R.H. "Laboratory Screening of Diesel Oxidation Catalyst and Validation with Vehicle Testing: The Importance of Hydrocarbon Storage." *Society of Automotive Engineers,* 962049 (1996).

Agarwal, Jugual K., and Gilmore J. Sem. 1980. CONTINUOUS FLOW, SINGLE-PARTICLE-COUNTING CONDENSATION NUCLEUS COUNTER. *Journal of Aerosol Science* 11, (4): 343-57.

AVL. "AVL 483 Micro Soot Sensor." December 2004. AVL.com. April 2010 <http://www.avl.com/wo/webobsession.servlet.go/encoded/YXBwPWJjbXMmcGFnZT12aWV3Jm1hc2s9ZG93bmxvYWQmbm9kZXRpdGxlaWQ9NDE2OTImbm9lbmNv_0AZGU9UERG.pdf>.

Bensaid, Samir, Daniele L. Marchisio, and Debora Fino. 2010. Numerical simulation of soot filtration and combustion within diesel particulate filters. *Chemical Engineering Science* 65, (1) (1/1): 357-63.

Burtscher, H. (2005). Physical characterization of particulate emissions from diesel engines: A review. *Journal of Aerosol Science*, *36*, 896–932.

Cadle, S. H., Groblicki, P. J., & Stroup, D. P. (1980). An automated carbon analyzer for particulate samples. *Analytical Chemistry*, *52*, 2201–2206.

Cantrell, B. K., and K. T. Whitby. 1978. Aerosol size distributions and aerosol volume formation for a coal-fired power plant plume. *Atmospheric Environment (1967)* 12, (1-3): 323-33.

Chase, Richard E., Gary J. Duszkiewicz, Joel F. O. Richert, Desmonia Lewis, and M. Matti Maricq and Ning Xu. "PM Measurement Artifact: Organic Vapor Deposition on Different Filter Media." *Society of Automotive Engineers,* 2004-01-0967, 2004.

Cooley, J. W. and J. W. Turkey. 1965 Maths Comput. 19, 297. An algorithm for the machine calculation of complex Fourier series.

Cooper, Barry J., and James E. Thoss. “Role of NO in diesel particulate emission control.” *Society of Automotive Engineers,* 890404. (1989).

Dabhoiwala, Rayomand H., John H. Johnson, and Jeffrey D. Naber. “Experimental Study Comparing Particle Size and Mass Concentration Data for a Cracked and Un-Cracked Diesel Particulate Filter.” *Society of Automotive Engineers,* 2009-01-0629, 2009.

Dekati Ltd. “DEKATI ETaPS Electrical Tailpipe PM Sensor.” August 2008. www.dekati.fi. January 2010 <http://dekati.com/cms/downloads>.

Diller, Timothy T., Matthew J. Hall, and Ronald D. Matthews. “Further Development of an Electronic Particulate Matter Sensor and Its Application to Diesel Engine Transients.” *Society of Automotive Engineers,* 2008-01-1065, 2008.

Dixon, John. “Measurement of Charge Distribution of Diesel Exhaust Aerosol Using a TDMA,” Master’s Thesis, University of Minnesota, 2007.

Dockery, D. W., Pope III, A., Xu, X., Spengler, J. D., Ware, J. H., Fay, M. E., Ferris, Jr. B. G. and Speizer, F. E. (1993) An association between air pollution and mortality in six U.S. cities. *J. Medicine* 329, 1753Ð1759.

Donaldson Company Inc. “Donaldson DPF and LTF Mufflers for the Highest Tailpipe PM Reduction.” March 2008. Donaldson.com. January 2010 <www.donaldson.com/en/exhaust/support/datalibrary/033834.pdf>.

Eastwood, Peter. 2000. *Critical topics in exhaust gas aftertreatment*. Baldock, Hertfordshire, England: Research Studies Press Ltd.

Ehara, Kensei, Charles Hagwood, and Kevin J. Coakley. 1996. Novel method to classify aerosol particles according to their mass-to-charge ratio—Aerosol particle mass analyser. *Journal of Aerosol Science* 27, (2) (3): 217-34.

Federal Register. (2010). Code of Federal Regulations, Title 40: Protection of Environment, Part 86: Control of Emissions from New and In-use Highway Vehicles and Engines. (Washington, DC: U.S. Government Printing Office).

Gheorghiu, V. 2006. Soot and particle sensor for onboard control of particle filters and control of the emissions of diesel engines presentation of the present state of development; russ- und partikelsensor fur onboard-uberwachung von partikelfiltern und kontrolle der emissionen von dieselmotoren vorstellung des aktuellen entwicklungsstands. *VDI Berichte*(1931): 839-50.

Gunn, Ross, and R. H. Woessner. 1956. Measurements of the systematic electrification of aerosols. Journal of Colloid Science 11, (3) (6): 254-9.

HEI (2003). *Revised analyses of time-series studies of air pollution and health*. Special Report, Boston, MA: Health Effects Institute.

Heywood, John B. 1988. *Internal combustion engine fundamentals*. New York: McGraw-Hill.

Howitt, John S., and Max R. Montierth. "Cellular ceramic diesel particulate filters." *Society of Automotive Engineers,* 810114. (1981).

Huntzicker, J. J., Johnson, R. L., Shah, J. J., & Cary, R.A. (1982). Analysis of organic and elemental carbon in ambient aerosol by a thermal-optical method. In: G. T.Wolff, & R. L. Klimisch (Eds.), *Particulate carbon: Atmospheric life cycle* NewYork: Plenum.

Johnson, Timothy V. "Review of Diesel Emissions and Control." *Society of Automotive Engineers,* 2010-01-0301. 2010.

Johnson, Timothy V. 2010. "Key developments in diesel emissions control and catalysts." *Platinum Metals Review*. 2010, 54, (1), 37–43.

Johnson, T. V. 2009. Review of diesel emissions and control. *International Journal of Engine Research* 10, (5): 275-85.

Jung, Heejung, and David B. Kittelson. 2005. Measurement of electrical charge on diesel particles. *Aerosol Science and Technology* 39, (12): 1129-35.

Kim, S. H., K. S. Woo, B. Y. H. Liu, and M. R. Zachariah. 2005. Method of measuring charge distribution of nanosized aerosols. *Journal of Colloid and Interface Science* 282, (1) (2/1): 46-57.

Kittelson, David B., David Y. H. Pui, and K. C. Moon. "Electrostatic Collection of Diesel Particles." *Society of Automotive Engineers,* 860009, 1986.

Kittelson, David B., and Nick Collings. "Origin of the Response of Electrostatic Particle Probes." *Society of Automotive Engineers,* 870476, 1987.

Kittelson, David B. 1998. Engines and nanoparticles: A review. *Journal of Aerosol Science* 29, (5-6): 575-88.

Kittelson, D., W. Watts, & J. Johnson. (2002). Diesel Aerosol Sampling Methodology. CRC E-43 Final Report, pp. 181 , NTIS Accession No. PB2003-102418l, available from CRC, Alpharetta, GA. Available at http://www.crcao.com/reports/recentstudies00-02/E-43%20Final%20Report.pdf

Kittelson, D.B., W.F. Watts, J.P. Johnson. "Ultrafine and nanoparticle emissions: a new challenge for internal combustion engine designers." Aerosols Handbook. CRC Press, 978-1-56670-611-7, 2005.

Kittelson, D. B., W. F. Watts, J. P. Johnson, C. Rowntree, M. Payne, S. Goodier, C. Warrens, et al. 2006. On-road evaluation of two diesel exhaust aftertreatment devices. *Journal of Aerosol Science* 37, (9) (9): 1140-51.

Knutson, E. O., and K. T. Whitby. 1975. Aerosol classification by electric mobility: Apparatus, theory, and applications. *Journal of Aerosol Science* 6, (6) (11): 443-51.

Hinds, William C. *Aerosol Technology: properties, behavior, and measurement of airborne particles*. New York: John Wiley & Sons Inc. 1999.

Lall, Anshuman Amit, and Sheldon K. Friedlander. 2006. On-line measurement of ultrafine aggregate surface area and volume distributions by electrical mobility analysis: I. theoretical analysis. *Journal of Aerosol Science* 37 (3) (3): 260-71.

Lighty, JoAnn Slama, John M. Veranth, and Adel F. Sarofim. 2000. Combustion aerosols: Factors governing their size and composition and implications to human health. *Journal of the Air and Waste Management Association* 50, (9): 1565-618.

Liu, Benjamin Y. H., and David Y. H. Pui. 1974. Equilibrium bipolar charge distribution of aerosols. *Journal of Colloid and Interface Science* 49, (2) (11): 305-12.

MacDonald, Scott, and Gerald M. Simon. "Development of a particulate trap system for a heavy-duty diesel engine." *Society of Automotive Engineers,* 880006 (1988).

Maricq, M. Matti. 2006. On the electrical charge of motor vehicle exhaust particles. *Journal of Aerosol Science* 37, (7) (7): 858-74.

Maricq, M. Matti. 2007. Chemical characterization of particulate emissions from diesel engines: A review. *Journal of Aerosol Science* 38, (11) (11): 1079-118.

MOON, KIL-CHOO. "CHARGING MECHANISM OF SUBMICRON DIESEL PARTICLES". Ph.D. diss., University of Minnesota ,1984. In Dissertations & Theses @ CIC Institutions [database on-line]; available from http://www.proquest.com (publication number AAT 8429469; accessed July 20, 2010).

Nieuwstadt, Michiel Van, and Dominic F. Trudell. "Diagnostics for diesel particulate filters." *Society of Automotive Engineers,* 2004-01-1422. (2004).

National Institute for Occupational Safety and Health. (1998). Elemental Carbon (Diesel Exhaust) 5040. Issue 2, January 15, 1998, 9 pp. in NIOSH Manual of Analytical Methods (NMAM), Fourth Edition, March 15, 1996. available at http://www.cdc.gov/niosh/docs/2003-154/pdfs/5040f3.pdf

Ochs, Thorsten, Henrik Schittenhelm, Andreas Genssle, and Bernhard Kamp. "Particulate matter sensor for on board diagnostics (OBD) of diesel particulate filters (DPF)." *Society of Automotive Engineers,* 2010-01-0307. (2010).

Park, Kihong, Feng Cao, David B. Kittelson, and Peter H. McMurry. 2003. Relationship between particle mass and mobility for diesel exhaust particles. *Environmental Science and Technology* 37, (3): 577-83.

Pope III, C. A., Burnett, R. T., Thurston, G. D., Thun, M. J., Calle, E. E., Krewski, D. et al. (2004). Cardiovascular mortality and long-term exposure to particulate air pollution. *Circulation*, *109*, 71–77.

Sinclair, David, and George S. Hoopes. 1975. A continuous flow condensation nucleus counter. *Journal of Aerosol Science* 6, (1): 1-7.

Stamatelos, A. M. 1997. A review of the effect of particulate traps on the efficiency of vehicle diesel engines. *Energy Conversion and Management* 38, (1) (1): 83-99.

Stone, Richard. *Introduction to Internal Combustion Engines*. Warrendale, PA : Society of Automotive Engineers, 1999.

TSI Incorporated. "Model 3090 Engine Exhaust Particle Sizer Spectromter." August 2006. www.tsi.com. February 2009.

TSI Incorporated. "Series 3080 Electrostatic Classifiers." April 2008. www.tsi.com. February 2009.

Vouitsis, E., Ntziachristos, L., & Samaras, Z. (2003). Particulate matter mass measurements for low emitting diesel powered vehicles: What's next?. *Progress in Energy Combustion Science*, *29*, 635–672.

Walton, Frank B., Edward K. Bueckert, Danny P. Archambault, Robert W. Kempster. "On-line measurement of diesel particulate loading in ceramic filters." *Society of Automotive Engineers,* 910324, 1991.

Wang, J., W. G. Shin, M. Mertler, B. Sachweh, H. Fissan, and D. Y. H. Pui. 2010. Measurement of nanoparticle agglomerates by combined measurement of electrical mobility and unipolar charging properties. *Aerosol Science and Technology* 44 (2): 97-108.

Wang, X.; Grose, M.; Caldow, R.; Swanson, J.; Watts, W.; Kittelson, D. Improvement of Engine Exhaust Particle Sizer Spectrometer for Engine Emissions Measurement. 28th AAAR Conference, Oct 26 – 30th, 2009, Minneapolis, Minnesota.

Wiedensohler, A., and H. J. Fissan. 1988. Aerosol charging in high purity gases. *Journal of Aerosol Science* 19, (7): 867-70.

Appendix A

Midpoint Mobilities, Midpoint Particle Diameters, and Fraction of Total Particle Concentration that Carries –6 to +6 Elementary Charges as a Function of Mobility

Particle Diameter Midpoint, nm	Mobility Midpoint $cm^2/v\text{-}s$	Fraction of Total Particle Concentration That Carries This Number (-6 to +6) of Charges												
		-6	-5	-4	-3	-2	-1	0	+1	+2	+3	+4	+5	+6
2.21	4.216E-01	0	0	0	0	0	0.0091	0.98268	0.0082	0	0	0	0	0
2.55	3.164E-01	0	0	0	0	0	0.0105	0.98007	0.0094	0	0	0	0	0
2.94	2.375E-01	0	0	0	0	0	0.0123	0.97691	0.0108	0	0	0	0	0
3.40	1.783E-01	0	0	0	0	0	0.0144	0.9731	0.0125	0	0	0	0	0
3.92	1.339E-01	0	0	0	0	0	0.0169	0.9685	0.0146	0	0	0	0	0
4.53	1.005E-01	0	0	0	0	0	0.0200	0.96297	0.0170	0	0	0	0	0
5.23	7.553E-02	0	0	0	0	0	0.0237	0.95634	0.0199	0	0	0	0	0
6.04	5.675E-02	0	0	0	0	0	0.0282	0.94842	0.0234	0	0	0	0	0
6.98	4.265E-02	0	0	0	0	0	0.0335	0.939	0.0275	0	0	0	0	0
8.06	3.207E-02	0	0	0	0	0	0.0398	0.92787	0.0323	0	0	0	0	0
9.31	2.412E-02	0	0	0	0	0	0.0472	0.9148	0.0380	0	0	0	0	0
10.75	1.815E-02	0	0	0	0	0	0.0559	0.89958	0.0445	0	0	0	0	0
12.41	1.367E-02	0	0	0	0	0	0.0659	0.88202	0.0520	0	0	0	0	0
14.33	1.030E-02	0	0	0	0	0	0.0774	0.86198	0.0606	0	0	0	0	0
16.55	7.767E-03	0	0	0	0	0	0.0903	0.83938	0.0703	0	0	0	0	0
19.11	5.862E-03	0	0	0	0	0	0.1047	0.81425	0.0810	0	0	0	0	0
22.07	4.429E-03	0	0	0	0	0.0004	0.1205	0.78618	0.0928	0.0002	0	0	0	0
25.48	3.351E-03	0	0	0	0	0.0008	0.1375	0.75588	0.1054	0.0004	0	0	0	0
29.43	2.539E-03	0	0	0	0	0.0015	0.1554	0.72334	0.1188	0.0009	0	0	0	0
33.98	1.927E-03	0	0	0	0	0.0029	0.1739	0.68883	0.1327	0.0017	0	0	0	0
39.24	1.465E-03	0	0	0	0	0.0051	0.1926	0.65272	0.1467	0.0029	0	0	0	0
45.32	1.116E-03	0	0	0	0	0.0084	0.2109	0.61545	0.1605	0.0048	0	0	0	0
52.33	8.532E-04	0	0	0	0	0.0131	0.2282	0.57755	0.1737	0.0075	0	0	0	0
60.43	6.539E-04	0	0	0	0	0.0195	0.2440	0.53969	0.1857	0.0111	0	0	0	0
69.78	5.030E-04	0	0	0	0	0.0278	0.2576	0.5026	0.1963	0.0157	0	0	0	0
80.58	3.885E-04	0	0	0	0.0012	0.0379	0.2686	0.46539	0.2050	0.0213	0.0005	0	0	0
93.06	3.014E-04	0	0	0	0.0026	0.0497	0.2766	0.4304	0.2115	0.0280	0.0012	0	0	0
107.46	2.350E-04	0	0	0.0001	0.0051	0.0628	0.2812	0.39728	0.2155	0.0356	0.0023	0	0	0
124.09	1.843E-04	0	0	0.0004	0.0091	0.0767	0.2825	0.36632	0.2169	0.0439	0.0041	0.0001	0	0
143.30	1.454E-04	0	0	0.0010	0.0146	0.0909	0.2804	0.33774	0.2158	0.0525	0.0066	0.0004	0	0
165.48	1.154E-04	0	0.0001	0.0023	0.0220	0.1047	0.2751	0.31172	0.2122	0.0612	0.0099	0.0008	0	0
191.10	9.227E-05	0	0.0003	0.0044	0.0309	0.1174	0.2671	0.28841	0.2065	0.0694	0.0139	0.0015	0.0001	0
220.67	7.428E-05	0.0001	0.0009	0.0077	0.0411	0.1285	0.2568	0.26786	0.1989	0.0768	0.0185	0.0026	0.0002	0
254.83	6.021E-05	0.0002	0.0019	0.0125	0.0522	0.1376	0.2448	0.25006	0.1898	0.0829	0.0234	0.0043	0.0005	0
294.27	4.914E-05	0.0005	0.0037	0.0187	0.0634	0.1443	0.2316	0.23483	0.1797	0.0873	0.0284	0.0064	0.0010	0.0001
339.82	4.036E-05	0.0012	0.0066	0.0262	0.0742	0.1486	0.2178	0.22184	0.1690	0.0901	0.0333	0.0090	0.0017	0.0002
392.42	3.336E-05	0.0025	0.0108	0.0348	0.0842	0.1505	0.2039	0.21058	0.1581	0.0910	0.0378	0.0120	0.0028	0.0005
453.16	2.772E-05	0.0046	0.0162	0.0440	0.0929	0.1503	0.1904	0.20035	0.1474	0.0903	0.0417	0.0151	0.0043	0.0009
523.30	2.315E-05	0.0079	0.0229	0.0534	0.1001	0.1481	0.1777	0.19035	0.1372	0.0883	0.0449	0.0183	0.0060	0.0016
604.30	1.941E-05	0.0123	0.0305	0.0623	0.1056	0.1445	0.1661	0.1797	0.1278	0.0854	0.0474	0.0214	0.0080	0.0025
697.83	1.634E-05	0.0180	0.0386	0.0705	0.1093	0.1398	0.1560	0.16748	0.1194	0.0821	0.0490	0.0242	0.0102	0.0036
805.84	1.380E-05	0.0246	0.0469	0.0775	0.1113	0.1345	0.1475	0.15282	0.1121	0.0789	0.0499	0.0266	0.0123	0.0050
930.57	1.169E-05	0.0319	0.0547	0.0831	0.1117	0.1289	0.1410	0.13491	0.1063	0.0763	0.0501	0.0286	0.0144	0.0064

Figure 23. Fraction of total particle concentration carrying a charge (-6 to +6)

Source: Gunn, 1956; Wiedensohler, 1988 as modified by TSI, 2008

Appendix B

The following data show the expected raw exhaust concentrations for the John Deere 4045 engine under various conditions. This data was complied from a number of different projects and was used to select the testing conditions to evaluate the failed DPF and Honeywell soot sensor.

Table 2. Engine conditions and summary dilution tunnel data for John Deere engine

Condition	Raw NO, ppm		Dilute NO, ppm		Dilution ratio		Tunnel temp, C	
	Avg	Std	Avg	Std	Avg	Std	Avg	Std
1400 RPM 450 Nm	705	2.5	2.88	0.04	245	3.93	47.3	0.16
1400 RPM 250 Nm	503	2.3	2.21	0.03	228	2.36	47.5	0.12
1400 RPM 100 Nm	290	1.0	1.31	0.01	221	1.39	47.4	0.15
1400 RPM 50 Nm	210	1.1	0.96	0.01	220	2.57	47.4	0.45
2400 RPM 450 Nm	434	2.1	1.95	0.01	222	1.64	47.0	0.16
2400 RPM 250 Nm	303	2.1	1.33	0.01	227	1.95	47.2	0.13
2400 RPM 100 Nm	188	0.7	0.83	0.01	226	1.95	47.2	0.18
2400 RPM 50 Nm	250	1.5	1.16	0.01	215	1.69	47.1	0.42
1000 RPM 250 Nm	854	2.6	3.60	0.02	237	1.39	47.0	0.15
1000 RPM 100 Nm	331	2.2	1.46	0.01	227	1.62	47.8	0.27
1000 RPM 50 Nm	250	1.5	1.16	0.01	215	1.69	47.1	0.42

Table 3. Estimates of mass obtained from the SMPS, EEPS, AVL and filter samples

Condition	SMPS, mg/m^3		EEPS, mg/m^3		AVL, mg/m^3		NIOSH filter, mg/m^3	
	Avg	Std	Avg	Std	Avg	Std	Avg	Std
1400 RPM 450 Nm	13.28	1.13	11.08	0.53	18.18	1.16	17.26	1.52
1400 RPM 250 Nm	11.50	1.12	8.84	0.29	10.79	0.59	10.55	1.17
1400 RPM 100 Nm	10.27	0.98	8.13	0.22	8.45	0.36	5.57	1.52
1400 RPM 50 Nm	4.78	0.56	3.66	0.12	3.58	0.19	3.24	0.5
2400 RPM 100 Nm	22.64	1.19	15.93	0.35	16.05	0.55		
2400 RPM 50 Nm	10.56	0.75	7.58	0.18	6.16	0.21		
1000 RPM 250 Nm	10.23	0.98	9.64	0.44	11.84	0.64		
1000 RPM 100 Nm	17.69	1.23	15.18	0.51	18.67	1.01		
1000 RPM 50 Nm	5.91	0.66	4.74	0.19	5.26	0.35		

Source: http://www.me.umn.edu/centers/cdr/reports/nioshrealtime.pdf

Table 4. Particle number and length data obtained from the SMPS, EEPS and EAD

Condition	SMPS, part/cm^3		EEPS, part/cm^3		EAD, mm/cm^3	
	Avg	Std	Avg	Std	Avg	Std
1400 RPM 450 Nm	3.53E+07	3.07E+06	3.66E+07	2.00E+04	431	14.8
1400 RPM 250 Nm	3.85E+07	2.94E+06	3.85E+07	8.53E+03	414	9.5
1400 RPM 100 Nm	4.22E+07	3.73E+06	3.98E+07	5.92E+03	405	7.7
1400 RPM 50 Nm	3.82E+07	4.69E+06	3.23E+07	2.84E+04	213	7.8
2400 RPM 450 Nm	4.96E+07	4.03E+06	4.64E+07	8.67E+03	460	11.4
2400 RPM 250 Nm	1.06E+08	4.23E+06	1.06E+08	1.39E+04	1093	17.1
2400 RPM 100 Nm	1.09E+08	4.77E+06	1.05E+08	1.19E+04	1010	14.4
2400 RPM 50 Nm	6.50E+07	3.90E+06	5.99E+07	7.08E+03	182	5.2
1000 RPM 250 Nm	1.92E+07	2.25E+06	2.23E+07	3.42E+03	293	9.6
1000 RPM 100 Nm	3.05E+07	2.36E+06	3.74E+07	6.25E+03	496	12.5
1000 RPM 50 Nm	1.84E+07	2.44E+06	1.82E+07	3.73E+03	182	5.2

Table 5. Volume concentrations calculated from SMPS and EEPS size distributions

Condition	SMPS, µm^3/cm^3		EEPS, µm^3/cm^3	
	Avg	Std	Avg	Std
1400 RPM 450 Nm	1.33E+04	1.13E+03	1.11E+04	5.33E+02
1400 RPM 250 Nm	1.15E+04	1.12E+03	8.84E+03	2.89E+02
1400 RPM 100 Nm	1.03E+04	9.79E+02	8.13E+03	2.21E+02
1400 RPM 50 Nm	4.78E+03	5.56E+02	3.66E+03	1.18E+02
2400 RPM 450 Nm	1.15E+04	1.19E+03	9.23E+03	3.10E+02
2400 RPM 250 Nm	2.85E+04	1.33E+03	2.00E+04	4.49E+02
2400 RPM 100 Nm	2.26E+04	1.19E+03	1.59E+04	3.52E+02
2400 RPM 50 Nm	1.06E+04	7.52E+02	7.58E+03	1.81E+02
1000 RPM 250 Nm	1.02E+04	9.80E+02	9.64E+03	4.42E+02
1000 RPM 100 Nm	1.77E+04	1.23E+03	1.52E+04	5.12E+02
1000 RPM 50 Nm	5.91E+03	6.57E+02	4.74E+03	1.87E+02

Appendix C

Figure 24. Drilling Holes

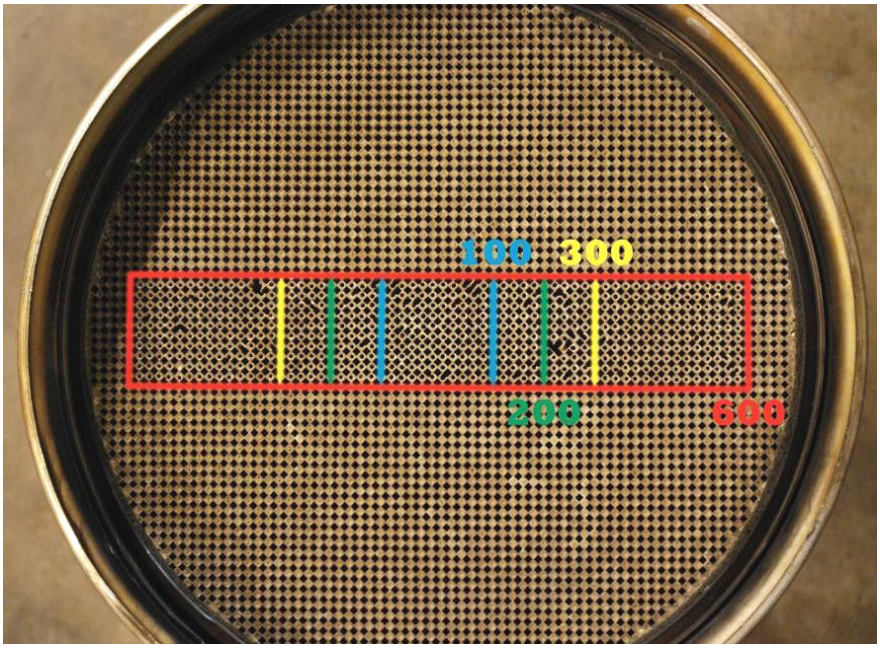

Figure 25. Hole Pattern

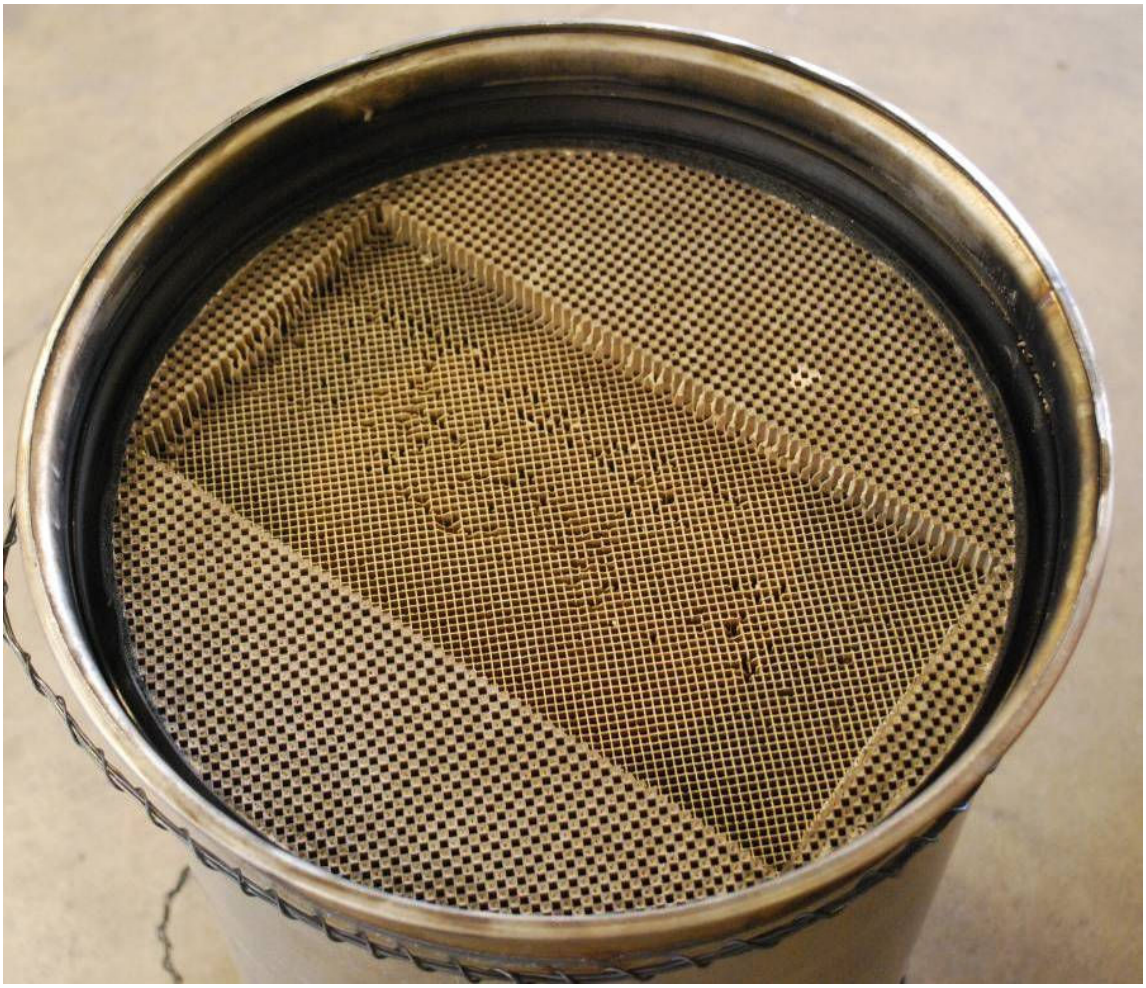

Figure 26. 1800 Milled

Appendix D

John Deere Engine
1400 RPM 350 Nm
No Aftertreatment

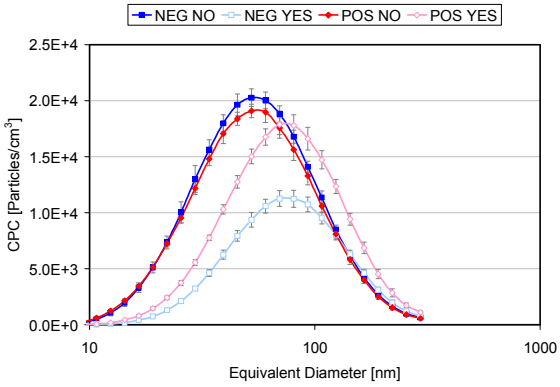

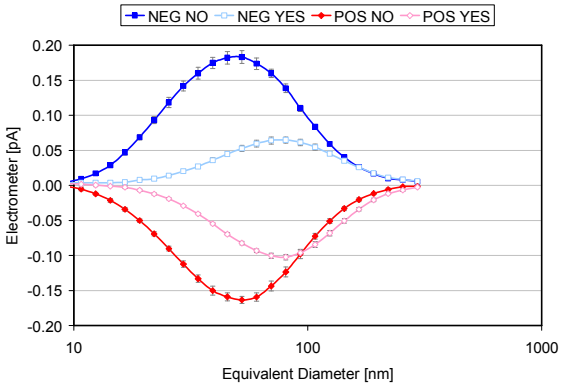

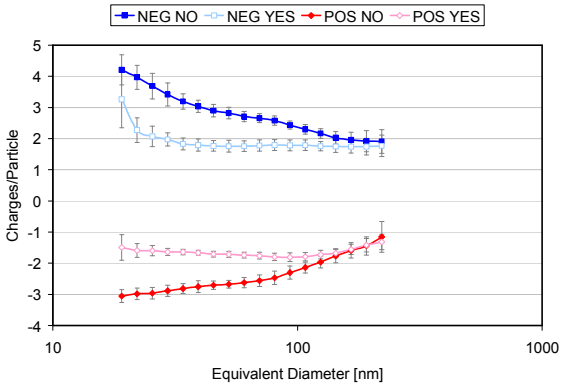

Isuzu Engine
1500 RPM 350 Nm
No Aftertreatment

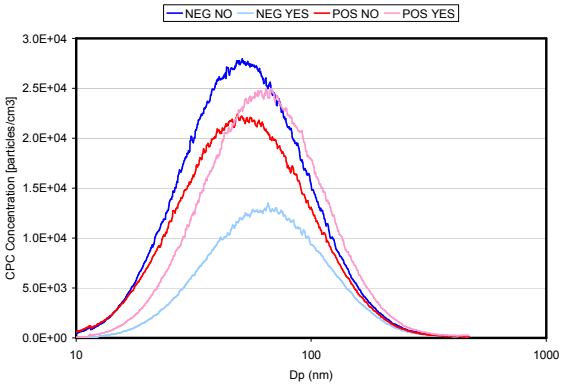

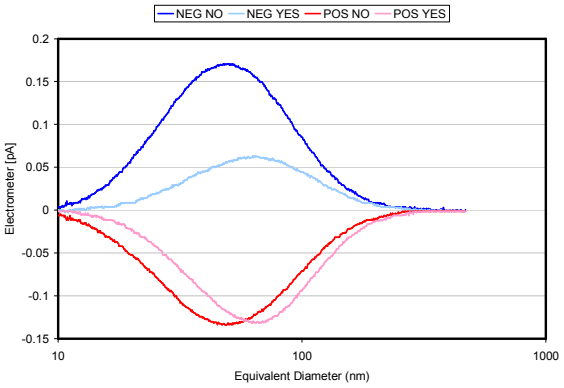

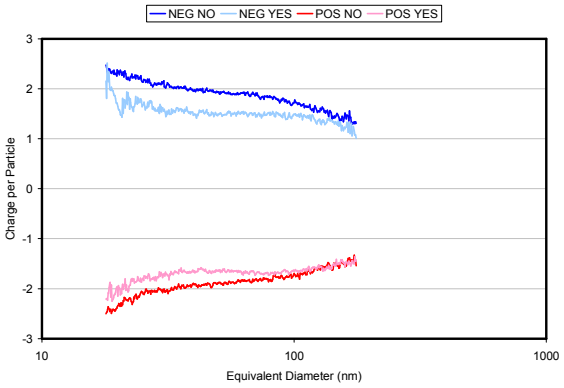

Isuzu Engine
1500 RPM 350 Nm
After Bypass Valve

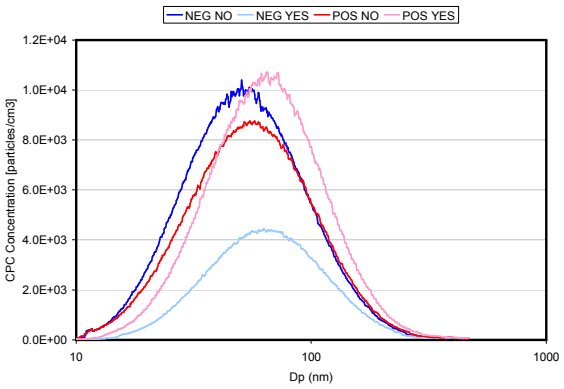

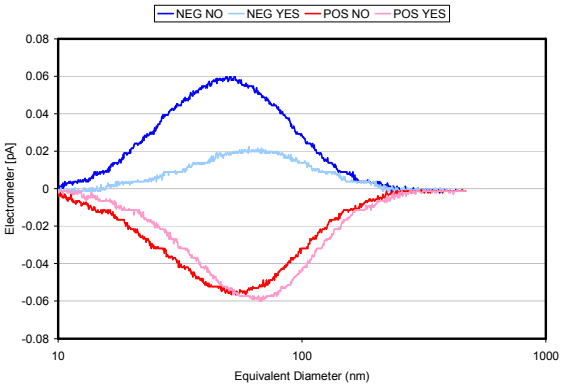

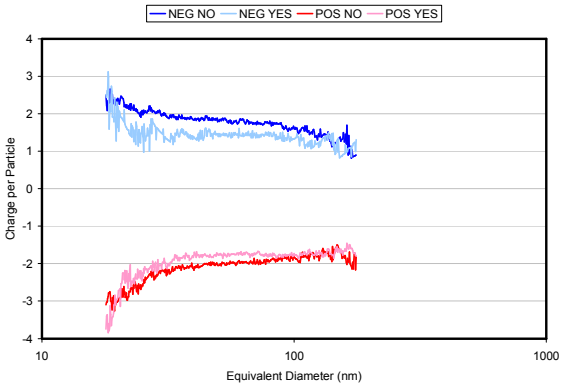

Isuzu Engine
1500 RPM 350 Nm
Failed DPF
1800 Milled